

ABSTRACT

Title of Thesis: **HIGHLY SIDEROPHILE ELEMENTS AND THE RHENIUM-OSMIUM SYSTEM IN CHONDRITIC COMPONENTS**

Greg Archer, M.S., 2012

Directed by: Professor Richard J. Walker, Geology

Chondritic meteorites and their components provide information about the early solar system, as well as processes that affected meteorite parent bodies post-accretion. The rare earth element (REE) abundances, highly siderophile element (HSE) abundances, Re-Os isotope systematics, Re isotopic composition, and Os isotopic composition were investigated in Allende chondritic components in order to: (1) classify several recently separated Allende calcium-aluminum-rich inclusions (CAIs) based on REE abundance patterns, (2) determine the abundances of six HSE (Re, Os, Ir, Ru, Pt, and Pd) in CAIs, chondrules, and matrix, and compare the different chondritic components, (3) further assess the magnitude and characteristics of open-system behavior on the Allende parent body using Re-Os of CAIs, chondrules, and matrix, (4) determine if the Re isotopic composition of CAIs was altered by cosmic ray interactions, and (5) investigate possible nucleosynthetic anomalies in CAIs.

HIGHLY SIDEROPHILE ELEMENTS AND
THE RHENIUM-OSMIUM SYSTEM IN
CHONDRITIC COMPONENTS

By

Greg Archer

Thesis submitted to the Faculty of the Graduate School of the
University of Maryland, College Park in partial fulfillment of
the requirements for the degree of
Master of Science
2012

Advisory Committee:

Professor Richard J. Walker, Chair
Associate Research Scientist Richard Ash
Professor James Farquhar

© Copyright by

Greg Archer

2012

Dedication

*To David and Erin Archer, my parents,
for encouraging me in all of my endeavors*

Acknowledgements

I would like to thank my advisor, Richard Walker, for guiding me through this project, and helping me shape every aspect of it. I appreciate his dedication, patience, and ability to impart knowledge to others. He has taught me many things, including laboratory techniques, how to run analytical instruments, and how to craft a scientific document. I would also like to thank my other committee members, Richard Ash and James Farquhar. Richard Ash provided insight into many aspects of my project through thoughtful discussion, and he helped me run analyses. He also provided several samples that I analyzed. James Farquhar provided valuable feedback on my project and thesis.

Researchers at the Smithsonian Institution were helpful collaborators with this project, and the Smithsonian Institution provided most of the samples analyzed by this study. Glenn MacPherson welcomed us to the extensive meteorite collection housed at the SI Museum of Natural History, and helped us select samples. Emma Bullock helped process those samples, and also provided X-ray maps of several of the samples. Both of them shared their knowledge of CAIs and passion for cosmochemistry with me.

Igor Puchtel provided a lot of help and advice to me in the lab. He showed a great deal of patience and thoughtfulness in helping me solve the challenges of my project. Bill McDonough, the current graduate director at UMd, not only gave me general advice about being a graduate student, but also contributed insight into aspects of my project. Jingao Liu, Katherine Birmingham, Mathieu Touboul, Emily Worsham, Miriam Galenas, Nick Sharp, and Lynette Pitcher helped me learn laboratory techniques as well as how to run analytical instruments. Several of them also listened to numerous practice

talks, and provided edits of written drafts of my thesis. James Day gave me valuable project advice as well as advice in the lab.

I would like to thank all of the graduate students for their moral support and all of the help they provided with my project. All of them have helped make UMd a great place to learn geoscience. I would also like to thank the staff of the department, Jeanne Martin, Sandy Romeo, Dorothy Brown, Todd Karwoski, Michelle Montero, Suzanne Martin, Joanna Patterson, June Sherer, and Bernadette Gatewood for all of their help. I would like to thank the entire faculty for the informative classes that they teach, the feedback that they provided, and their advice in the lab. I would especially like to thank our former department chair, Mike Brown, as well as our current department chair, Roberta Rudnick.

Finally, I would like to thank my family, David, Erin, James, John, and Mary for their love and support, as well as my girlfriend, Julia.

Table of Contents

Dedication	ii
Acknowledgements	iii
Table of Contents.....	v
List of Tables	vii
List of Figures	viii
Chapter 1: Introduction.....	1
1.1 Chondritic Meteorites.....	1
1.2 Chondritic Components	2
1.2.1 Calcium-Aluminum-Rich Inclusions	2
1.2.2 Chondrules and Matrix	6
1.2.3 Summary	8
1.3 Trace Elements in Chondritic Components.....	8
1.3.1 Highly Siderophile Elements	8
1.3.2 Rhenium-Osmium Systematics	12
1.3.3 Rhenium Isotopic Composition	14
1.3.4 Nucleosynthetic Anomalies in Trace Elements of Calcium-Aluminum-Rich Inclusions	15
1.4 Purpose of Study.....	17
Chapter 2: Samples	19
2.2 First Suite CAIs	21
2.3 Second Suite CAIs.....	21
2.4 Allende Chondrules and Matrix.....	27
Chapter 3: Methods.....	29
3.2 Highly Siderophile Elements and the Re-Os System in Chondritic Components	31
3.3 Nucleosynthetic Anomalies in Trace Elements of CAIs.....	34
Chapter 4: Results	36
4.1 Classification of Second Suite CAIs.....	36
4.2 Highly Siderophile Elements in Chondritic Components	39
4.2.1 Highly Siderophile Elements in Calcium-Aluminum-Rich Inclusions	39
4.2.2 Highly Siderophile Elements in Chondrules	44
4.2.3 Highly Siderophile Elements in Matrix.....	45
4.3 Rhenium-Osmium Systematics of Allende Components	46
4.4 Rhenium and Osmium Isotopic Composition	49

Chapter 5: Discussion	54
5.1 Rare Earth Elements	54
5.1.1 Condensation of REE in CAIs	54
5.1.2 Minor Differences of REE Patterns in Second Suite CAIs Compared to Previous Results	54
5.2 Highly Siderophile Elements in Chondritic Components	55
5.2.1 Highly Siderophile Elements in CAIs	55
5.2.2 Refractory HSE-rich Precursor	56
5.2.3 Two HSE-bearing Components	57
5.2.4 Highly Siderophile Elements in Matrix	59
5.3 Rhenium-Osmium Systematics in Chondritic Components	60
5.3.1 Analytical Issues	61
5.3.2 Early Solar System Processes	63
5.3.3 Late Stage Open-System Behavior	64
5.3.4 Higher Degree of Variability in Smaller Samples	66
5.3.5 Modeling Re-Os Systematics of Bulk Allende using Components	66
Chapter 6: Synthesis	68
References	72

List of Tables

Table 1: Concentrations of REE in Second Suite CAIs	36
Table 2: HSE abundances of CAIs, chondrules, and matrix	41
Table 3: Re-Os systematics of CAIs, chondrules and matrix.....	50
Table 4: Os isotopic composition of standards and Allende CAIs	53

List of Figures

Figure 1: Condensation sequence of material from a cooling gas of solar composition.....	3
Figure 2: Typical REE patterns of CAIs for different groups normalized to bulk CI chondrites	6
Figure 3: Representative HSE patterns of CAIs, normalized to CI chondrites	10
Figure 4: HSE patterns for several ordinary chondrite components	11
Figure 5: Re-Os systematics of CAIs and chondrite groups replotted from Becker <i>et al.</i> (2001)	13
Figure 6: Nuclides of the Os region, showing s, r, p and radiogenic Os.....	16
Figure 7: Os nucleosynthetic anomalies for acid resistant phases of Murchison, Allende, and Tagish Lake	17
Figure 8: Photograph of Allende including chondrules and calcium-aluminum-rich inclusions	20
Figure 9: Location of Allende meteorite fall showing strewnfield	20
Figure 10: X-ray map of Allende CAI 3507 19B65	22
Figure 11: X-ray map of Allende CAI 3507 5A8.....	23
Figure 12: X-ray map of Allende CAI 3507 3A7	24
Figure 13: X-ray map of Allende CAI 3507 7B75	25
Figure 14: X-ray map of Allende CAI 3507 9A30.....	26
Figure 15: X-ray map of Allende CAI 3507 18B61	27
Figure 16: Measured concentrations of BIR-1 from this study compared with GeoReM accepted BIR-1 values.....	30
Figures 17(a-d): Chondrite-normalized REE patterns of 6 Allende CAIs.....	38
Figure 18: Chondrite-normalized HSE abundances of First Suite CAIs	42
Figure 19: Chondrite-normalized HSE abundances of Second Suite CAIs....	42
Figure 20: Pd vs. Os abundances, in ppb, of non-group II Allende CAIs	43
Figure 21: Pt vs. Os abundances, in ppb, of non-group II Allende CAIs	43
Figure 22: Chondrite-normalized HSE abundances of Allende & Chainpur Chondrules	45
Figure 23: Chondrite-normalized HSE abundances of Allende matrix	46
Figure 24: Re-Os systematics of Allende CAIs.....	51
Figure 25: Re-Os systematics of Allende CAIs.....	51
Figure 26: Re-Os systematics of chondrules and Allende matrix	52
Figure 27: Δ_{Os} vs. $^{187}\text{Re}/^{188}\text{Os}$ of Allende CAIs, chondrules, and matrix	52
Figure 28: Os isotopic composition of Allende CAIs	53
Figure 29: Model Re-Os systematics of bulk Allende	67

Chapter 1: Introduction

1.1 Chondritic Meteorites

Chondritic meteorites are the most primitive known meteorites, and are, therefore, key sources of information about the early Solar System. They are conglomerate-like rocks with three main components: chondrules, matrix, and refractory inclusions. Refractory inclusions are further subdivided into calcium-aluminum-rich inclusions (CAIs) and amoeboid olivine aggregates. It is currently believed that these components formed in the solar nebula, and then coalesced to form parent bodies that were not subsequently differentiated (e.g., Wadhwa & Russell, 2000).

There are two general models describing the formation of chondrites in the early Solar System. Both models are based on observations related to short-lived (now extinct) radionuclides (SLRs). One model proposes that chondritic components formed via heating events which were caused by shock waves (Alexander, 2001; Desch and Connolly, 2002; Desch *et al.*, 2005; Morris and Desch, 2010). For this model, the short-lived radionuclides were generated in other stellar environments and injected into the early solar nebula (Vanhala & Boss, 2002). The putative shock waves may have been generated by X-ray flares, bow shocks caused by planetesimals, or gravitational instabilities (Desch *et al.*, 2005). The second model, termed the X-wind model, hypothesizes that CAI and chondrule precursors were transported to <0.1 AU from the Sun, melted, and then were transported out to 2-3 AU (Shu *et al.*, 1997; 2001). This model corresponds to production of short-lived radionuclides within our Solar System by irradiation near the protosun (Gounelle *et al.*, 2001).

1.2 Chondritic Components

1.2.1 Calcium-Aluminum-Rich Inclusions

Calcium-aluminum-rich inclusions are sub-millimeter to centimeter-sized clasts in chondrites that are found in nearly all types of chondrites, except for Ivuna-type chondrites (CI). They have been studied extensively, and are among the most important sources of information about the early Solar System. Using ^{207}Pb - ^{206}Pb isotope systematics, Bouvier and Wadhwa, (2010) established an age of $4,568.67 \pm 0.17$ Myr for a CAI from the CV3 meteorite NWA 2364. This is the oldest age for any known object that formed in the Solar System (Bouvier and Wadhwa, 2010). Because of their antiquity, CAIs preserve evidence about chemical and isotopic heterogeneity present during the earliest stages of Solar System evolution (Clayton *et al.*, 1976; Niederer *et al.*, 1981; Chen *et al.*, 2010; Brennecka *et al.*, 2011; Burkhardt *et al.*, 2011). Furthermore, they may shed light on postformational processes, such as early cosmic ray interactions and later stage open-system behavior.

The mineralogy of CAIs closely resembles the first phases that are predicted, through thermodynamic calculations, to condense from the solar nebula at temperatures above ~ 1400 K (Grossman, 1972) (Figure 1). Thus, they likely represent the first solids that condensed from the cooling solar nebula (Gray *et al.*, 1973; MacPherson *et al.*, 1995; Amelin *et al.*, 2002; Bouvier and Wadhwa, 2010). The most common phases in CAIs are Ca|Al|Ti|Mg-oxides and silicates, including melilite ($\text{Ca}_2(\text{Al},\text{Mg})(\text{Si},\text{Al})_2\text{O}_7$), spinel (MgAl_2O_4), perovskite (CaTiO_3), hibonite ($\text{CaAl}_{12}\text{O}_{19}$), Ca-pyroxene ($\text{Ca}(\text{Mg},\text{Fe},\text{Al})(\text{Si},\text{Al})_2\text{O}_6$), anorthite ($\text{CaAl}_2\text{Si}_2\text{O}_8$), and forsterite (Mg_2SiO_4). Although there is some pressure dependence on the condensation of minerals from the solar nebula,

pressure plays only a minor role at the low total pressures of 10^{-3} to 10^{-6} bars, which are believed to be representative of the solar nebula at the time of CAI formation (Grossman & Clark, 1973; Yoneda & Grossman, 1995). Excepting major element chemistry, temperature is the most influential factor in the condensation sequence in this environment. It is, therefore, generally accepted that some CAIs are non-igneous and are instead direct nebular condensates, while other CAIs may have crystallized from partially to completely molten droplets (melted condensates), and may have experienced episodes of melting as well as later alteration after becoming incorporated into their parent bodies (MacPherson, 2003).

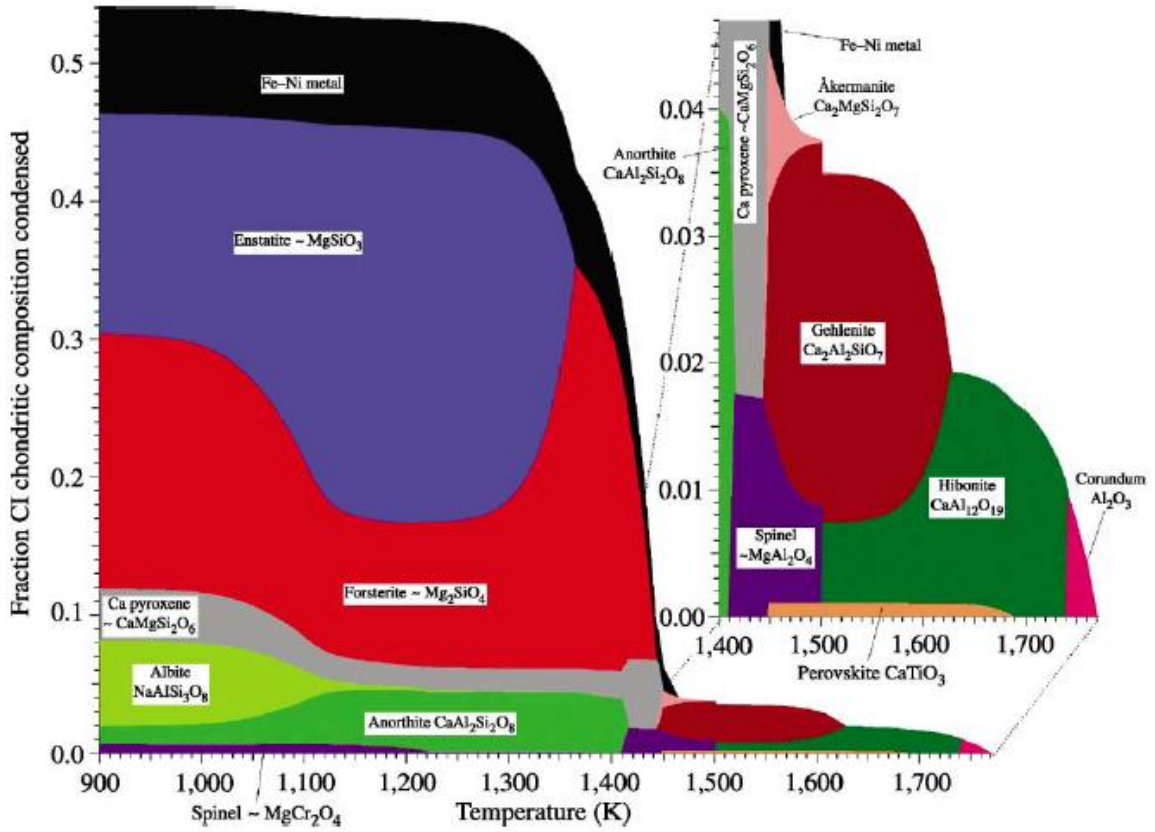


Figure 1: Condensation sequence of material from a cooling gas of solar composition. Figure taken from Davis & Richter (2003). Calculations taken from Grossman (1972).

Calcium-aluminum-rich inclusions have two main accepted classification schemes. The first scheme, originally proposed by Grossman (1975), designates CAI *types* based on petrographic characteristics, including grain size and the modal abundances of the major mineralogical components, fassaite and melilite. Of coarse-grained CAIs, there are three types, melilite-rich type A, the relatively more fassaite-rich type B, and the plagioclase-rich type C (Wark, 1987). The fine-grained variety of CAI is spinel-rich (Grossman, 1975). For a more detailed review of this classification scheme, the reader is referred to Brearley & Jones (1998).

Calcium-aluminum-rich inclusions have also commonly been classified into *groups*, based on the bulk relative abundances of their rare earth elements (REE) (Figure 2), which reflect their elemental volatilities. The fractionation of REE based on volatility is consistent with CAIs being subject to evaporation-condensation processes (Ireland & Fegley, 2000). Rare earth elements were condensed in conjunction with the major CAI minerals and incorporated into different silicate phases depending on crystallochemical factors. Diverse phases within CAIs have distinct patterns based on the affinities of REE for each of the phases. For example, Mason & Martin (1974) reported that the REE patterns of pyroxene and melilite are complementary within a CAI. Within pyroxene, the REE, with the exception of La and Eu, are enriched compared to the concentrations found in melilite. Furthermore, melilite has a relative enrichment in Eu, whereas pyroxene has a relative depletion (Mason & Martin, 1974).

The REE patterns of groups I, III, V, and VI are enriched by a factor of approximately 20 compared to bulk chondrites, whereas their relative abundances are essentially unfractionated relative to bulk chondrites, resulting in an approximately flat

REE pattern (Figure 2). Only small anomalies in Eu and Yb, the most volatile REE, distinguish these different groups of CAIs (Mason and Martin, 1977). Group I CAIs are characterized by slightly positive Eu anomalies, but no Yb anomalies. Group III CAIs are characterized by negative Eu and Yb anomalies. Group V CAIs have completely unfractionated REE patterns. Group VI CAIs are characterized by positive Eu and Yb anomalies (Mason and Taylor, 1982). Fractionations among REE for groups I, III, V, and VI are believed to be a result of complete condensation from a solar gas (e.g., Martin & Mason, 1974). The term “group IV CAIs” has fallen out of favor and the popular consensus is that CAIs previously termed “group IV CAIs” should not be classified as CAIs.

In contrast to groups I, III, V, and VI, group II patterns are highly fractionated, with large negative anomalies, relative to average group I, III, V, and VI patterns (~20 x CI), in both the most refractory REE, Gd, Tb, Dy, Ho, Er, Lu, as well as Eu und Yb, the most volatile (Mason and Taylor, 1982) (Figure 2). Group II patterns are interpreted as the result of fractional condensation (Boynton, 1975; Davis & Grossman, 1979). Fractional condensation refers to a process whereby an ultrarefractory component, containing the most refractory REE, is removed by condensation and the residual gas condenses with the remaining REE, except for Eu and Yb, which are the most volatile. The refractory phase responsible for removing the refractory REE was most likely hibonite (MacPherson & Davis, 1994). It should be noted that some unusual CAIs do not fit well within either classification scheme; however, these CAIs are rare (Allen *et al.*, 1980; Wark, 1986; Caillet, 1994).

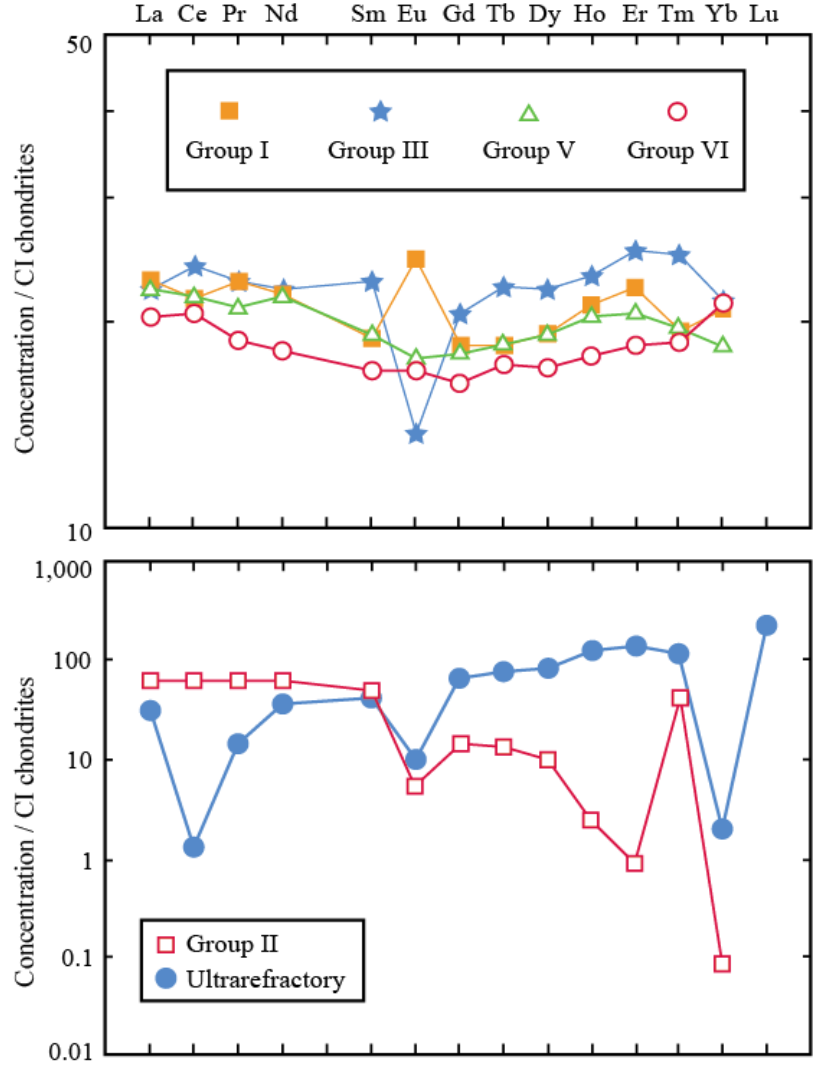


Figure 2: Typical REE patterns in CAIs for different groups as normalized to bulk CI chondrites. Figure reproduced from MacPherson (2003). Data from Mason and Taylor (1982); Ireland *et al.* (1988); Davis *et al.* (1982).

1.2.2 Chondrules & Matrix

Chondrules are millimeter to centimeter sized spherical silicate clasts present in all chondritic meteorites, except for CI chondrites. Based on ^{207}Pb - ^{206}Pb isotope systematics, most chondrules are believed to have formed 2-3 million years after CAIs (Amelin *et al.*, 2002; Krot *et al.*, 2005; Connelly, J. *et al.*, 2008; Bouvier & Wadhwa,

2010). Thus, they can provide information about the conditions of the early Solar System shortly after CAI formation. They are composed primarily of olivine, pyroxene and feldspar or feldspathic glass (Taylor, 2001). Chondrules were formed when chondrule precursor materials aggregated, were flash heated, and then cooled (e.g., Grossman *et al.*, 1988). There are several proposed mechanisms for flash heating chondrules, including collisional events between planetary bodies (Urey & Craig, 1953; Sanders, 1996), X-ray flares during the Sun's early active stage (Shu *et al.*, 2001), shock waves (e.g., Wood, 1963; Desch & Connolly, 2002), and nebular lightning (Desch & Cuzzi, 2000). As chondrules are present in the same bodies as CAIs, they can potentially provide complementary information about post chondrite formation behavior.

Matrix is defined by Scott *et al.* (1988) as “the fine-grained, predominantly silicate material, interstitial to macroscopic, whole or fragmented, entities such as chondrules, inclusions and large isolated minerals (i.e., silicate, metal, sulfide and oxide) grains.” Roughly 40% of the CV3 chondrite Allende is comprised of matrix material. Phases found in CV3 matrices include olivine, high-Ca pyroxene, nepheline, sodalite, pentlandite, troilite, magnetite and Fe-Ni metal (Scott *et al.*, 1988). Matrix materials are relatively complex in comparison to CAIs and chondrules. Matrix can contain phases that condensed from the solar nebula, presolar grains, as well as fragments of chondrite inclusions such as chondrules and matrix. Matrix material is fine-grained (commonly 50–100 nm in diameter), porous, and highly permeable. Matrix, consequently, is more susceptible to aqueous alteration in the parent body than other chondritic components (Scott *et al.*, 1988).

1.2.3 Summary

Chondritic components are a key to understanding early Solar System conditions and processes, as they were the first materials to form from the solar nebula. Additionally, they formed by different processes and under different conditions with respect to one another, but were somehow incorporated into the same parent bodies. Processes that acted upon parent bodies, as opposed to processes that only affected certain chondritic components can also therefore be assessed by comparing different components within the same parent body.

1.3 Trace Elements in Chondritic Components

1.3.1 Highly Siderophile Elements

The highly siderophile elements (HSE) condensed from the solar nebula in conjunction with the minerals that formed the Solar System's earliest solids. These minerals were collected into early formed chondritic components including CAIs and chondrules. The HSE are so named because of their strong affinity to Fe-metal rather than silicates. Because of this property, they are useful in assessing the relationship between metals and silicates in chondritic components and other materials. The HSE considered in this study are Re, Os, Ir, Ru, Pt, and Pd.

Rhenium and Os in metallic form are extremely refractory, with 50% condensation temperatures of 1817 K and 1808 K, respectively at 10^{-4} atm; whereas, of these HSE, Pd is the least refractory, with a 50% condensation temperature of only 1324 K at 10^{-4} atm (Lodders, 2003). Because HSE condensation temperatures overlap with the condensation temperatures of chondritic components, HSE are particularly useful in

evaluating condensation and evaporation processes of the early Solar System. Prior studies have reported that the HSE abundances in group I, III, V, and VI CAIs are generally \sim 20 x CI bulk chondrites, except for Pd, which is typically enriched by only \sim 2 x CI abundances (Wänke *et al.*, 1974; Mason & Taylor, 1982) (Figure 3). The HSE abundances of group II CAIs are much lower, with reported concentrations typically around 0.5 x CI. The lower group II abundances are consistent with fractional condensation (Figure 3), which is also evidenced by the highly fractionated REE abundances in these CAIs (MacPherson, 2003).

Although the REE in all CAI groups and HSE in non-group II CAIs are enriched relative to bulk chondrites, these element groups are concentrated in different phases. In CAIs, the HSE are mainly contained in refractory, metal-rich alloys that formed by condensation in the early solar nebula. For example, Ru and Os form hexagonal close packed alloys, whereas Pt and Ir form face-centered cubic alloys (Palme & Wlotzka, 1976). Submicroscopic alloys, which are typically dispersed among the major minerals in CAIs, are the dominant carriers of refractory siderophile elements. However, where present in some CAIs, opaque assemblages, so called “Fremdlinge,” are also highly enriched in refractory siderophile elements and can contribute a significant portion of the overall HSE budget of the bulk CAI (Palme *et al.*, 1993). In comparison, the REE are incorporated into the crystal lattices of the major silicate phases.

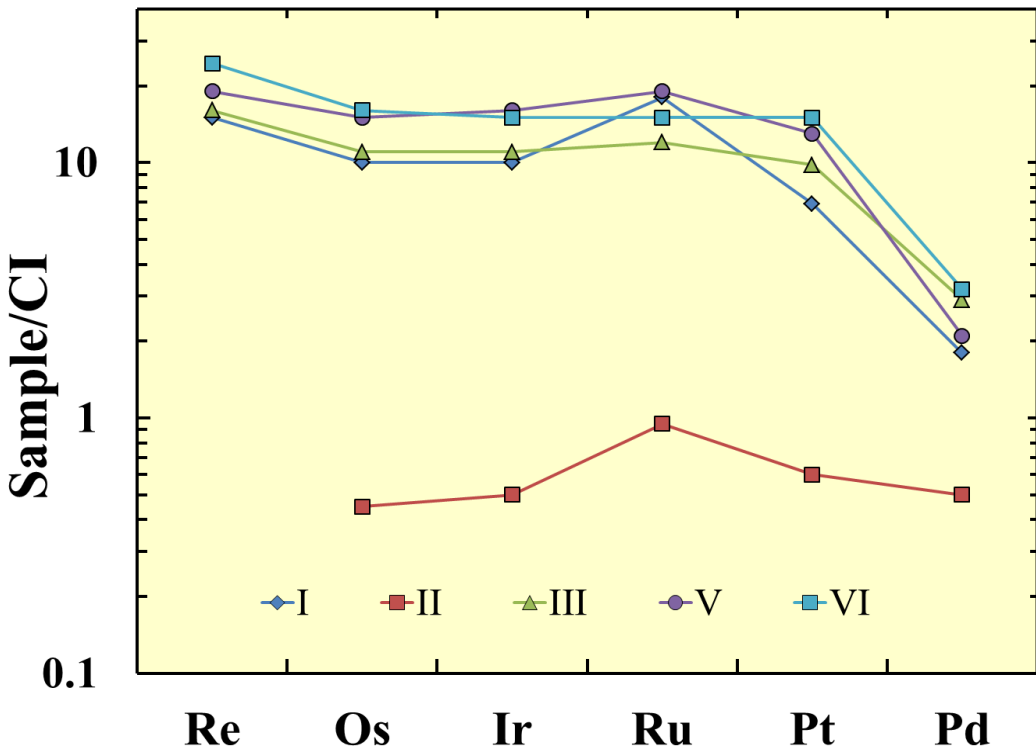


Figure 3: Representative HSE patterns, normalized to CI chondrites, ordered by 50% condensation temperature, decreasing from left to right, for all five groups of CAIs. Data taken from Mason and Taylor (1982).

Only a handful of studies have examined HSE abundances in chondrules, with the majority reporting only Ir data (e.g., Rubin & Wasson, 1987). Further, several studies have examined the HSE abundances of metal in chondrules from CR chondrites (Connolly *et al.*, 2001; Humayan *et al.*, 2010). Due to differences in HSE concentrations between metal grains on the interior and exterior of chondrules, these studies concluded that the metal in chondrules studied formed via reduction and volatilization. Walker *et al.* (2002) reported Re and Os abundances in Allende chondrules. Their data indicated movement of Re and/or Os into or out of chondrules. Horan *et al.* (2009) examined magnetic and nonmagnetic fractions of chondrules extracted from ordinary chondrites.

They showed that nonmagnetic fractions from chondrules have highly fractionated HSE patterns, with large depletions in Pd, and a low Re/Os (Figure 4). They also reported that, in contrast, separated metal fractions were characterized by elevated but flat CI-normalized abundance patterns (Figure 4). The high abundances of HSE in the nonmagnetic fractions were interpreted to indicate that there had been incomplete equilibration with surrounding metal. If there had been complete equilibration with the surrounding metal, the abundances of HSE in nonmagnetic fractions would have been lower because HSE have such an extreme affinity for Fe-metal.

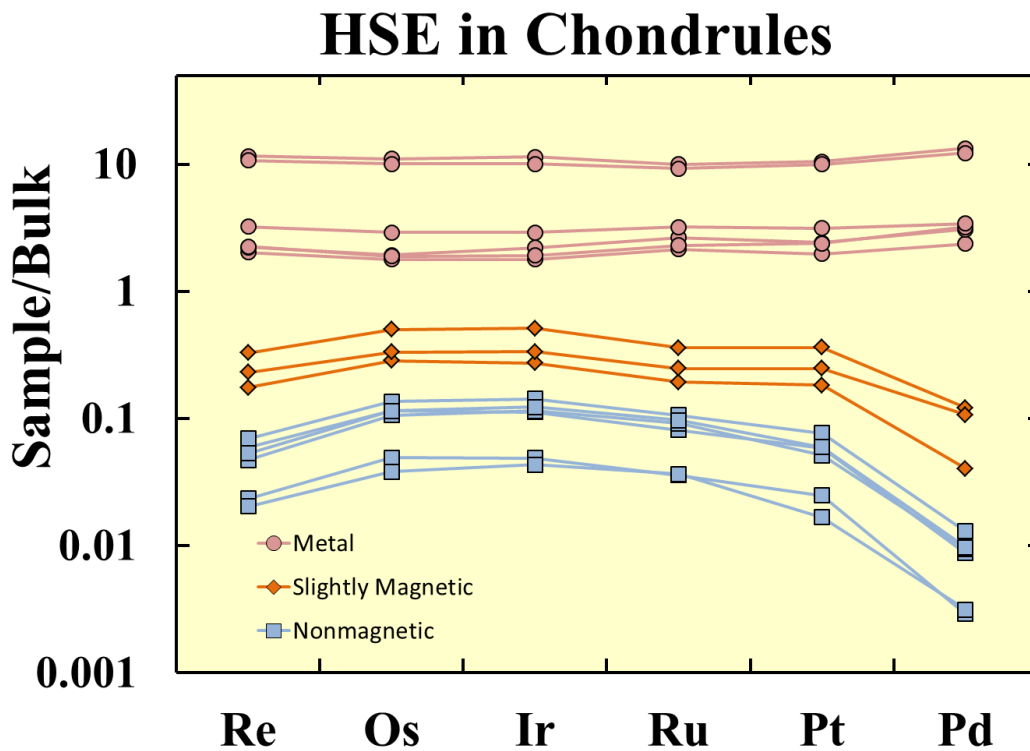


Figure 4: HSE patterns ordered by 50% condensation temperature, decreasing from left to right, for several ordinary chondrite components (taken from ordinary chondrite Ochansk) including chondrule metal and nonmetal fractions. Figure replotted from Horan *et al.* (2009).

It is also important to understand the contributions of matrix material to the overall HSE budget of Allende. There are even fewer HSE data for matrix material than chondrule data. Becker *et al.* (1999) and Walker *et al.* (2002) reported Re-Os data for several Allende matrix fractions. Like chondrules, the data indicated that Re and/or Os were mobilized into or out of matrix material after formation.

1.3.2 Rhenium-Osmium Systematics

The rhenium-osmium isotopic system, in which ^{187}Re decays via negatron emission to ^{187}Os ($\lambda=1.666 \times 10^{-11} \text{ a}^{-1}$), has the potential to date processes that affected the HSE in chondritic components (Becker *et al.*, 2001). As chondritic components are the oldest known materials to have condensed from the solar nebula, they would be expected to plot on a primordial, 4.568 Ga Re-Os reference isochron, if they escaped post-formation processes that affected Re-Os systematics.

Becker *et al.* (2001) showed that eight out of a total of sixteen analyzed Allende CAIs analyzed by that study did not plot within analytical uncertainties of a primordial 4.568 Ga reference isochron (Figure 5). They reviewed several possible explanations for CAIs deviating from the primordial isochron. The possibilities include open-system behavior, chemical differentiation processes in the early solar nebula, primordial heterogeneities of the solar nebula, and analytical issues. Becker *et al.* (2001) considered the most probable explanation to be late-stage open system behavior of the Allende parent body. They reasoned that the other possibilities were unlikely culprits for the non-isochronous behavior of some CAIs. Chemical differentiation is an unlikely option as any chemical differentiation via condensation and evaporation processes would have to

first fractionate Re/Os in the early Solar System. Then, the Re/Os system would have to remain closed for hundreds of thousands or millions of years, and a second fractionation event would have to return the Re/Os back to the observed near-chondritic Re/Os observed today. Analytical issues are unlikely as the blanks measured by Becker *et al.* (2001) were not sufficiently high to alter the apparent Re-Os systematics, and their digestion technique was deemed by them to be the most effective and reliable one available to access HSE bearing phases. The isotopic composition of other Os isotopes did not indicate mixing of nonsolar Os (and therefore primordial heterogeneities).

Based on the data from one CAI, 3529-41, Becker *et al.* (2001) calculated a 1614 ± 39 Ma internal isochron (Figure 5). They argued that the data for this CAI provides age constraints for the event that caused open-system behavior in the Allende parent body.

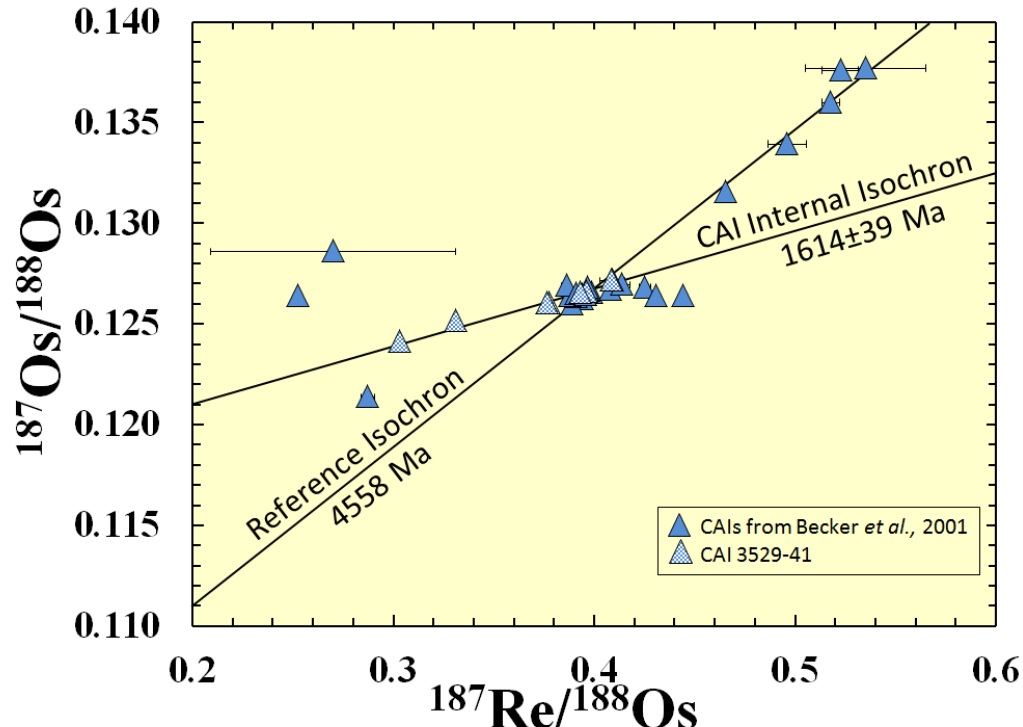


Figure 5: Re-Os systematics of CAIs replotted from Becker *et al.* (2001).

If Re-Os systematics of Allende CAIs plot off of a primordial isochron because of open system behavior on the parent body, then other components, like chondrules and the matrix of Allende, might also be characterized by similar behavior. Becker *et al.* (1999) and Walker *et al.* (2002) reported data for several Allende chondrules and matrix that do not plot on a primordial isochron.

1.3.3 Re Isotopic Composition

Another possible mechanism that could cause CAIs to plot off of a primordial isochron, not considered by Becker *et al.* (2001), is cosmic ray interaction. This process involves energetic particles from the early Sun irradiating CAIs and inducing nuclear reactions that change the isotopic composition of elements present in the CAIs. In calculating the $^{187}\text{Re}/^{188}\text{Os}$ for an isochron plot of CAIs, the $^{185}\text{Re}/^{187}\text{Re}$ is assumed to be a natural constant, and the abundance of ^{187}Re is simply derived from the concentration of Re in the sample. However, if the Re isotopic composition has been altered, this is not a valid assumption.

There is evidence that spallation reactions caused by cosmic rays were responsible for generating certain short-lived radioisotopes in the early Solar System (e.g., ^{10}Be) (MacPherson *et al.*, 2003; Wielandt *et al.*, 2012). The isotopes ^{185}Re and ^{187}Re have moderately high neutron capture cross-sections of 112.1 and 76.7 barns, respectively (Mughabghab, 2003). Neutron capture cross-sections are a measure of the probability that a nuclear reaction will occur for a particular nuclide. Thus, it is possible that cosmic ray interactions between the early Sun and CAIs modified the isotopic composition of Re in CAIs, changing their $^{185}\text{Re}/^{187}\text{Re}$.

1.3.4 Nucleosynthetic Anomalies in Trace Elements of Calcium-Aluminum-Rich Inclusions

As the earliest formed materials in our Solar System, CAIs can be (and have been previously) used to study the degree of homogenization of presolar grains that accumulated from multiple stellar sources in the early Solar System. These grains had their genesis in different stellar environments which were dominated by different nucleosynthetic processes, giving them highly variable and distinct isotopic compositions. They were injected into the early Solar System and became incorporated into the first materials to form in the early Solar System. If presolar material was not well mixed in the solar nebula, then isotopic anomalies would exist in early Solar System material.

Burkhardt *et al.* (2011) reported that Mo in Allende CAIs shows nucleosynthetic anomalies with several samples of CAIs having enrichments in *r*-process (rapid neutron capture) and one sample having depletion in *s*-process (slow neutron capture) Mo. Chen *et al.* (2010) found nucleosynthetic anomalies in Ru in Allende CAIs. Several of the samples analyzed showed depletions in ^{100}Ru , an isotope only produced by *s*-process, indicating an *s*-process deficit. Brennecka *et al.* (2011) found enrichments in *r*-process Ba (^{135}Ba and ^{137}Ba), deficits in *r*-process Nd, and deficits in *r*-process and *p*-process Sm in Allende CAIs. All of these studies illustrate that CAIs preserve evidence for isotopic anomalies that can be attributed to different nucleosynthetic processes.

Nucleosynthetic anomalies in Os have been reported for chondritic materials including acid leached fractions of bulk chondrites (e.g., Yokoyama *et al.*, 2007). The seven isotopes of osmium, ^{192}Os , ^{190}Os , ^{189}Os , ^{188}Os , ^{187}Os , ^{186}Os , ^{184}Os , are produced by different nucleosynthetic processes, including *r*-, *s*-, and *p*-process nucleosynthesis

(Figure 6). Stellar environments like asymptotic giant branch (AGB) stars and supernova explosions produce different process-dependent nuclides in different proportions depending on the nucleosynthetic processes that are prevalent within them.

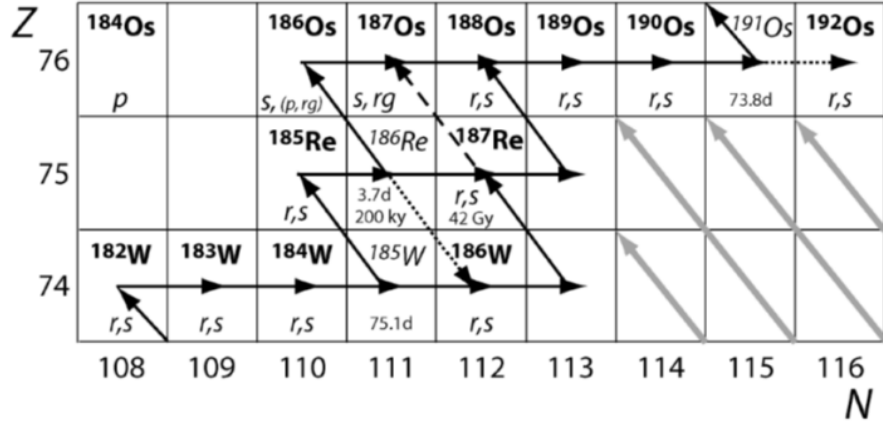


Figure 6: Nuclides of the Os region, showing s, r, p and radiogenic (rg) Os. From Reisberg *et al.* (2009)

Deviations from accepted Solar System values of Os are reported in εOs units.

The equation to determine εOs for a particular isotope is as follows:

$$\varepsilon^x\text{Os} = ((^x\text{Os}/^{189}\text{Os})_{\text{sample}} / (^x\text{Os}/^{189}\text{Os})_{\text{solar}} - 1) \times 10^4$$

^xOs is the isotope being considered. The data are typically displayed in an $\varepsilon^x\text{Os}$ vs. isotope graph (Figure 7). Yokoyama *et al.* (2007) used this method for displaying Os data taken from different fractions of bulk chondrites. Data can also be presented by $\varepsilon^{186}\text{Os}^i$ vs. $\varepsilon^{188}\text{Os}$ and $\varepsilon^{190}\text{Os}$ vs. $\varepsilon^{188}\text{Os}$ graphs, in which positive $\varepsilon^{186}\text{Os}^i$, $\varepsilon^{188}\text{Os}$, and $\varepsilon^{190}\text{Os}$ indicate *s*-process enrichment, and negative $\varepsilon^{186}\text{Os}^i$, $\varepsilon^{188}\text{Os}$, and $\varepsilon^{190}\text{Os}$ indicate *r*-process enrichment. Using this method, deviations in Os can be compared to astrophysical models for the mixing of presolar material in the solar nebula.

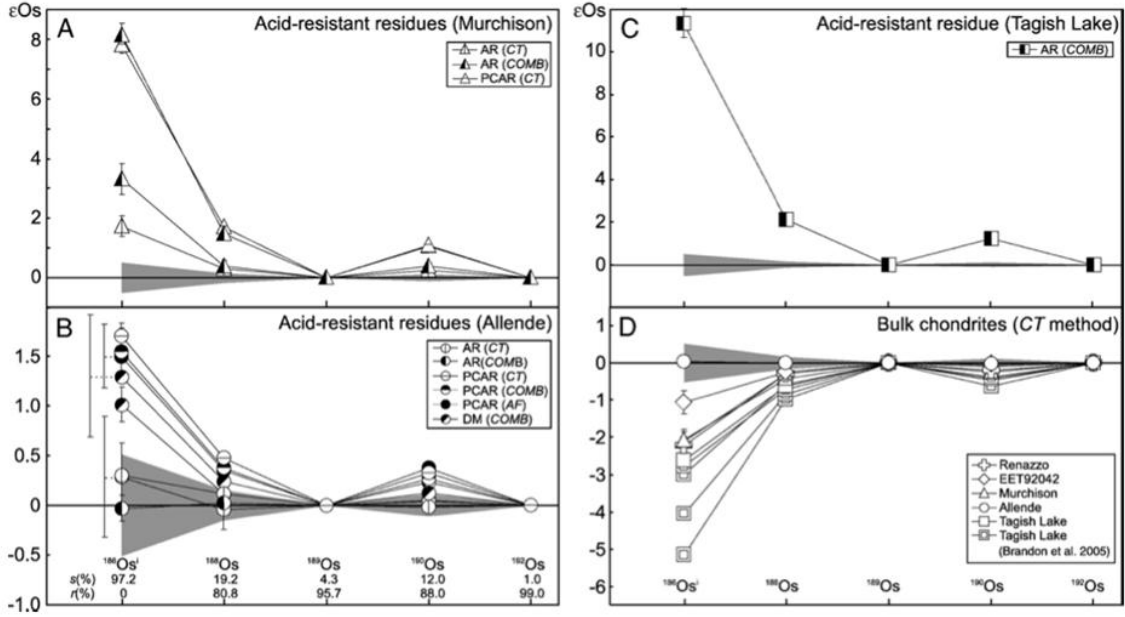


Figure 7: Os nucleosynthetic anomalies in $\epsilon^{80/82}\text{Os}$ notation for acid resistant phases of Murchison (A), Allende (B) and Tagish Lake (C), and for bulk carbonaceous chondrites decomposed by carius tube digestion (D). Shaded zones are the $\pm 2\sigma$ reproducibilities of nine bulk carbonaceous chondrites decomposed by alkaline fusion. Taken from Yokoyama *et al.* (2007).

Yokoyama *et al.* (2009) analyzed Os in CAIs in an attempt to ascertain whether or not nucleosynthetic anomalies for Os are present. Within uncertainty, their data did not support the existence of such anomalies in CAIs. However, their data only consisted of measurements from two CAIs, so the data set was not extensive enough to confidently rule out the existence of nucleosynthetic anomalies.

1.4 Purpose of Study

In this study, the REE abundances, highly siderophile element abundances, Re-Os isotope systematics, Re isotopic composition, and Os isotopic composition were investigated in Allende chondritic components in order to: (1) classify several recently

separated Allende CAIs based on REE abundance patterns, (2) determine the abundances of six HSE (Re, Os, Ir, Ru, Pt, and Pd) in CAIs, chondrules, and matrix, and compare the different chondritic components, (3) further assess the magnitude and characteristics open-system behavior on the Allende parent body using Re-Os of CAIs, chondrules, and matrix, (4) determine if the Re isotopic composition of CAIs was altered by cosmic ray interactions, and (5) investigate possible nucleosynthetic anomalies in CAIs.

Chapter 2: Samples

2.1 The Allende Meteorite

The Allende meteorite fell in Chihuahua, Mexico, on February 8th, 1969 (Clark *et al.*, 1970). The timing of the fall of Allende, shortly before the landing of Apollo 11 on the Moon, was fortuitous in that many research institutions had been recently equipped with state-of-the-art equipment for geochemical analyses of samples soon to be returned from the Moon. From a strewnfield of about 300 km², over two tons of material was collected. Allende is the largest recorded stony meteorite fall in terms of areal extent and recovered material (Figure 9) (Clark *et al.*, 1970). These factors have led to Allende being the most extensively studied meteorite in history. Individual pieces of this meteorite range in mass from approximately 1 g to 110 kg (Clark *et al.*, 1970).

Allende is classified as a CV3 (carbonaceous, Vigarano-like) meteorite (Figure 8). On average, Allende consists of approximately 9% calcium-aluminum-rich inclusions, 3% amoeboid olivine aggregates, 43% chondrules, 41% matrix and 3% opaque minerals (McSween, 1977), but the proportions of these components can vary greatly among different pieces. Additionally, Allende is grouped in the oxidized subclassification of CVs (McSween, 1977).



Figure 8: Photograph of Allende including chondrules and calcium-aluminum-rich inclusions. Ruler scale is in centimeters. (Photo credit: Randy L. Korotev, Washington University in St. Louis)



Figure 9: Location of Allende meteorite field (red) showing size of strewnfield. Figure reproduced from Clark *et al.* (1970).

2.2 First Suite CAIs

Fragments of CAIs, including 3529-Z, 3520-40, and 3529-41, from a suite of over 40 CAIs that was separated from Allende in the early 1970's, were initially characterized. This suite will be referred to as "First suite CAIs". Calcium-aluminum-rich inclusions 3529-Z, 3520-40, and 3529-41 have been previously characterized for REE classification as well as HSE elements (Mason & Taylor, 1982). Two CAIs from this suite, 3529-41 and 3529-40, have been previously characterized for Re-Os systematics (Becker *et al.*, 2001). Only CAI 3529-35 had not been previously characterized for REE, HSE, or Re-Os systematics. The data collected in this study are compared with the data presented by the previous studies listed above in the results and discussion sections.

2.3 Second Suite CAIs

Fragments of 6 individual CAIs selected from a suite of CAIs that was recently separated from Allende by researchers at the Smithsonian Institution were characterized for REE abundances, HSE abundances, and Re-Os systematics (this suite will be referred to as "Second suite of CAIs"). These CAIs are 3507-19B65, 3507-5A8, 3507-3A7, 3507-7B75, 3507-9A30, and 3507-18B61. They have not been previously characterized for REE, HSE, or Re-Os systematics. A description of the second suite CAIs follows.

Note: Sample descriptions and X-ray maps of CAIs were provided by Emma Bullock of the Smithsonian Institute

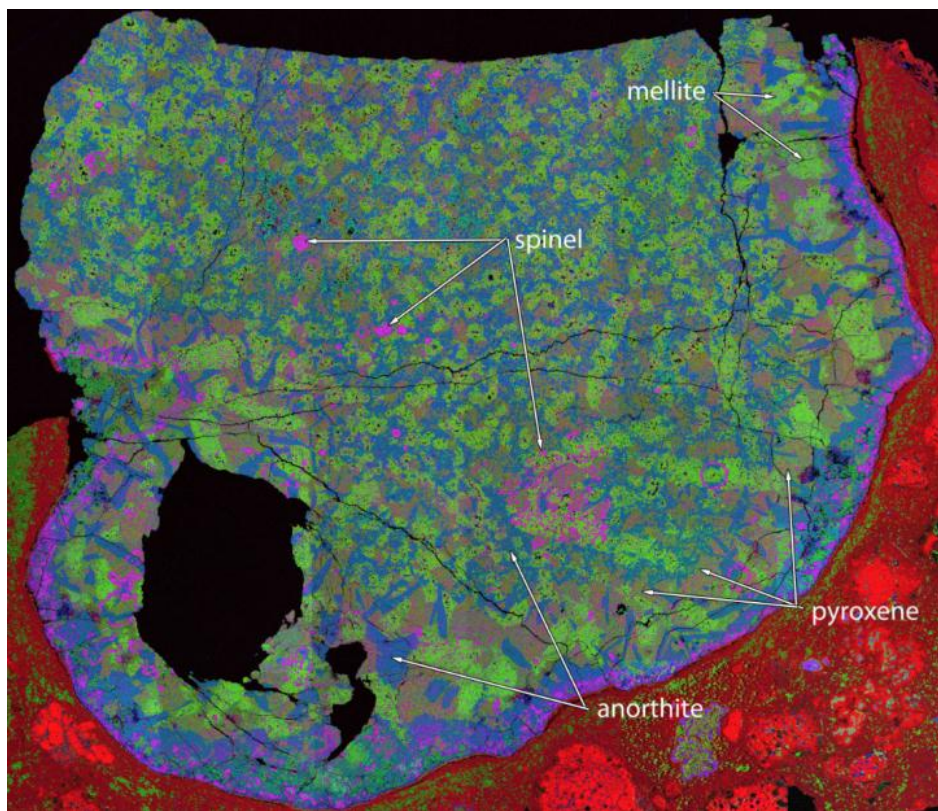


Figure 10: X-ray map of Allende CAI 3507 19B65. Provided by Emma Bullock of the Smithsonian Institute.

Allende 3507 19B65: This is a large (~2.5cm diameter), rounded Type C CAI (Figure 10). Lacy melilite grains (comp $\text{Ak}_{72}\text{-}\text{Ak}_{77}$) are porous, and have undergone some secondary alteration to grossular/andradite. Pyroxene (Al_2O_3 13-21 wt%; TiO_2 3-6 wt%) occurs throughout the inclusion. Fine-grained spinel occurs as frambooidal masses and palisades, and is generally low in FeO (<2 wt%), with the exception of a grain near the rim (6 wt% FeO). Anorthite is abundant, and forms both interstitial masses and well-formed prismatic crystals that show little evidence of secondary alteration (<0.5 wt% Na_2O). The rim of the inclusion consists of coarse-grained anorthite and melilite, bounded by a Wark-Lovering rim of spinel and pyroxene.

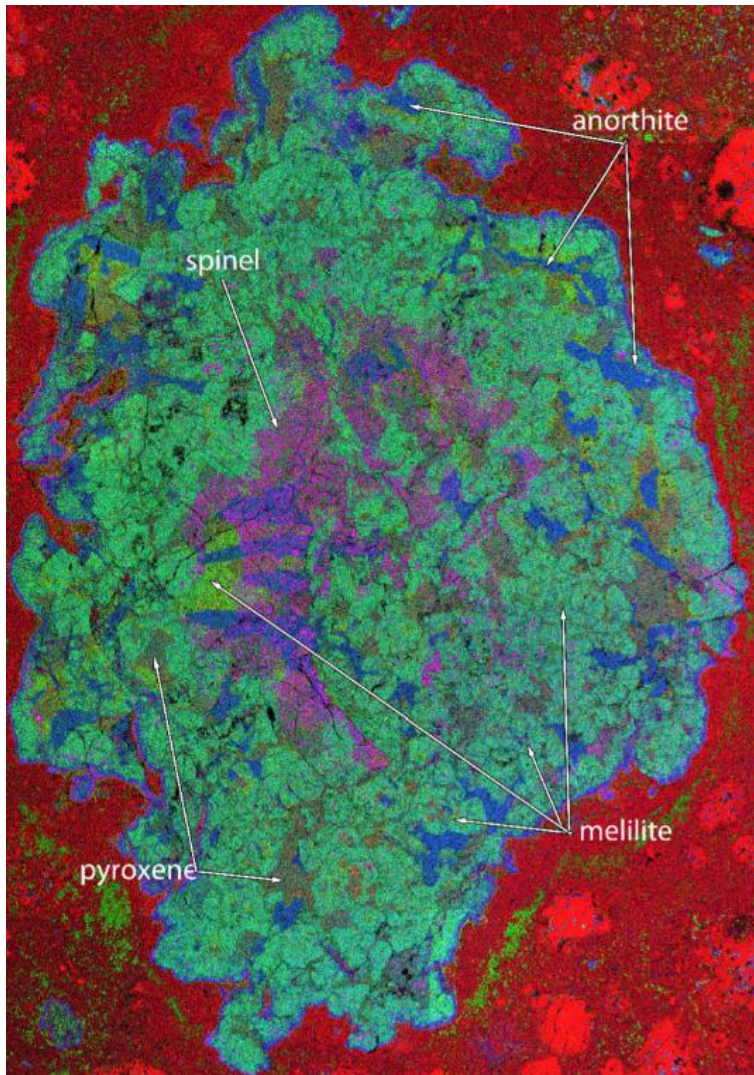


Figure 11: X-ray map of Allende CAI 3507 5A8. Provided by Emma Bullock of the Smithsonian Institute.

Allende 3507 5A8: This is a large (~2cm diameter), irregular Type B CAI (Figure 11). The inclusion comprises strongly zoned melilite (Ak_{20-60}), Ti-bearing pyroxene (TiO_2 3-10 wt%), and euhedral anorthite laths (<0.1 wt% Na_2O). Abundant fine-grained spinel is concentrated in the core of the inclusion, and is poikolitically included in melilite, pyroxene and anorthite. The Wark-Lovering rim of the inclusion consists of fine-grained layers (~10-20 μm) of nepheline, spinel, forsterite and pyroxene.

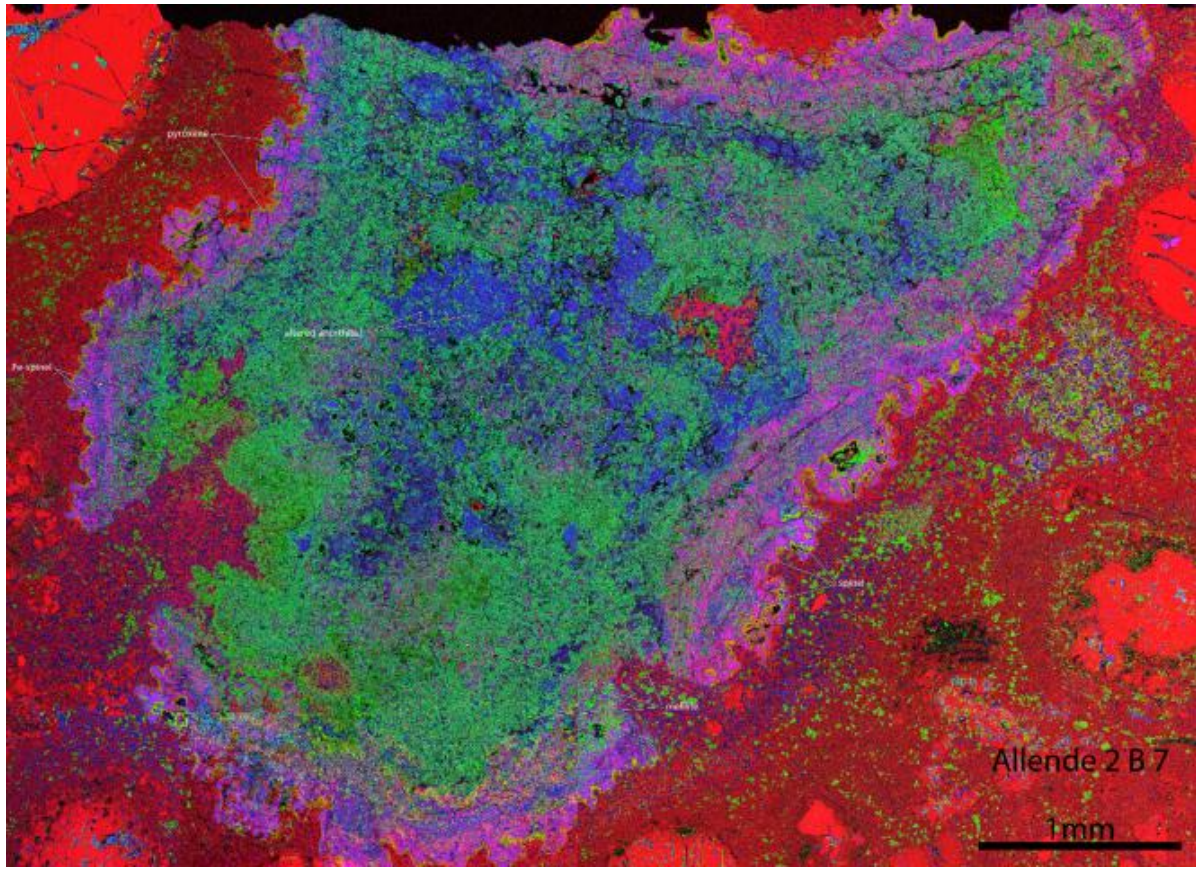


Figure 12: X-ray map of Allende CAI 3507 3A7. Provided by Emma Bullock of the Smithsonian Institute.

Allende 3507 3A7: This is a fine-grained, irregular inclusion that shows evidence of alteration to secondary phases such as nepheline, andradite and hedenbergite (Figure 12). Fine-grained spinel ($5\text{-}10 \mu\text{m}$) is dispersed throughout the inclusion, and a rim of fine-grained spinel that coarsens towards the outside of the inclusion is present. The fine-grained nature of this inclusion makes it difficult to obtain reliable electron probe data. The CAI is surrounded by Wark-Lovering rim of low-Ti pyroxene.

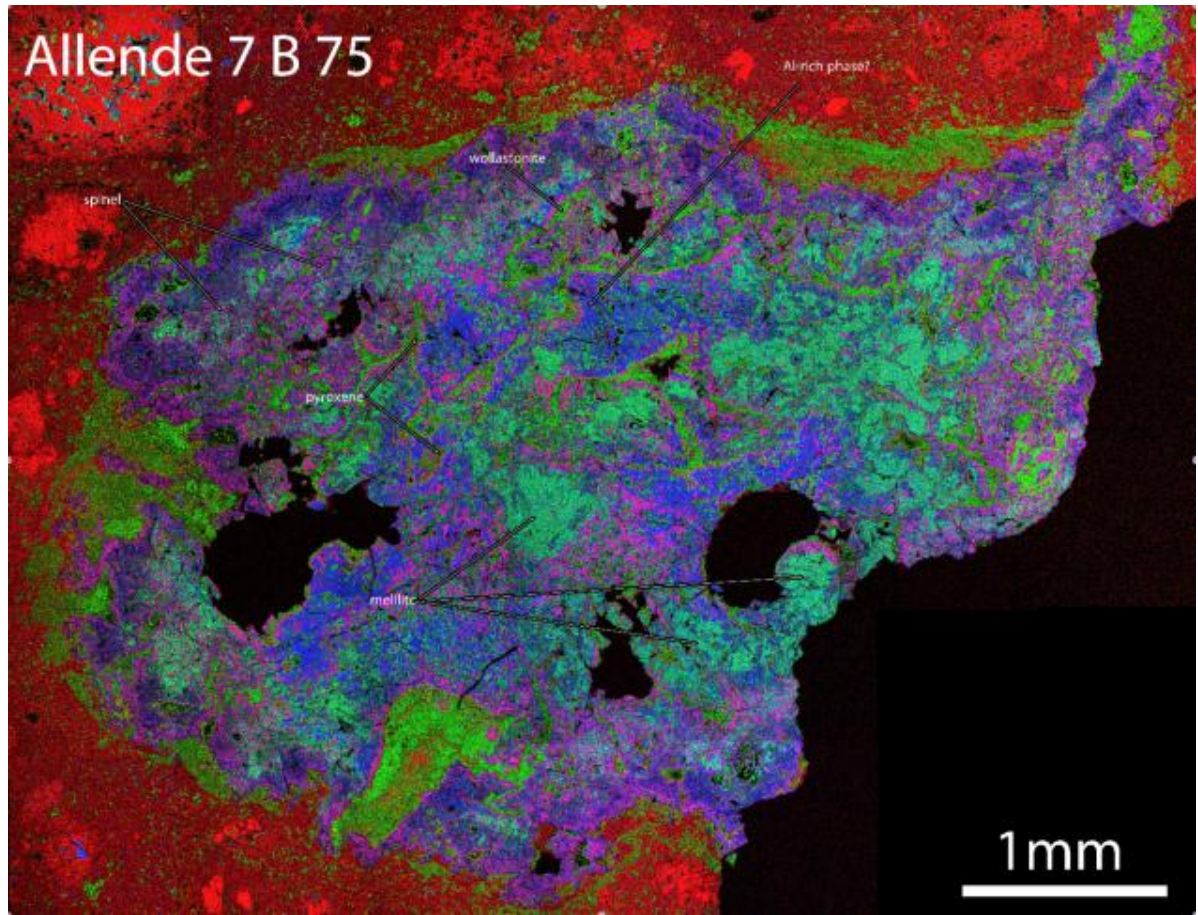


Figure 13: X-ray map of Allende CAI 3507 7B75. Provided by Emma Bullock of the Smithsonian Institute.

Allende 3507 7B75: This is a highly altered Type B CAI, ~0.5cm in diameter (Figure 13). It contains several large vesicles, and some of these have been in-filled by matrix. Melilite in 7B75 is strongly gehlenitic (Ak_{10-16}). Spinel is abundant, ranges from fine- to coarse-grained, and contains 2-10 wt% FeO. Anorthite shows alteration to nepheline. Wollastonite, hedenbergite and low-Ti (<1 wt%) pyroxene are present. The inclusion shows no evidence of a Wark-Lovering rim, and it appears that calcium has been leached from the inclusion into the surrounding matrix.

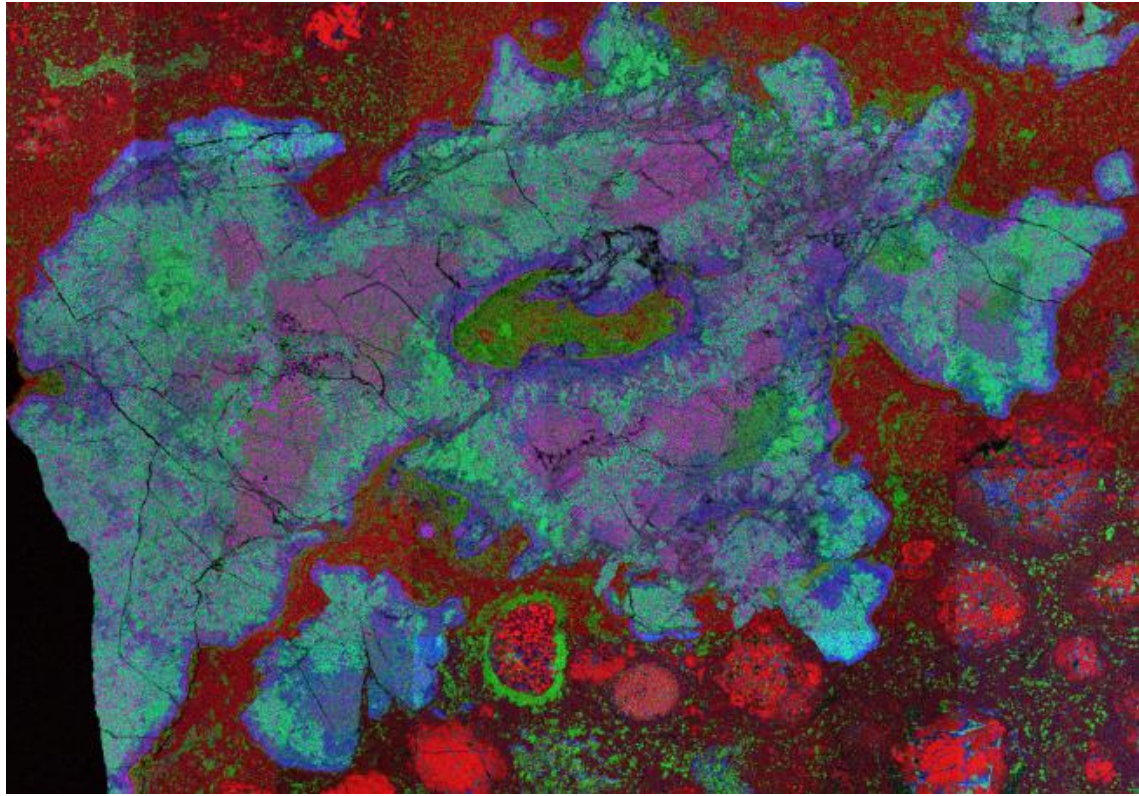


Figure 14: X-ray map of Allende CAI 3507 9A30. Provided by Emma Bullock of the Smithsonian Institute.

Allende 3507 9A30: This inclusion is a large, irregular compact Type A CAI with a sinuous shape (Figure 14). Melilite ranges from Ak_{5-35} , and poikolitically encloses abundant fine-grained spinel. Pyroxene also poikolitically encloses abundant spinel, to the extent where obtaining good electron probe data of the pyroxene grains is difficult. The limited data available suggest a TiO_2 content of ~10 wt%. The inclusion shows evidence of secondary alteration, particularly around the edges of the grain. The inclusion has a Wark-Lovering rim that consists of spinel, olivine and pyroxene.

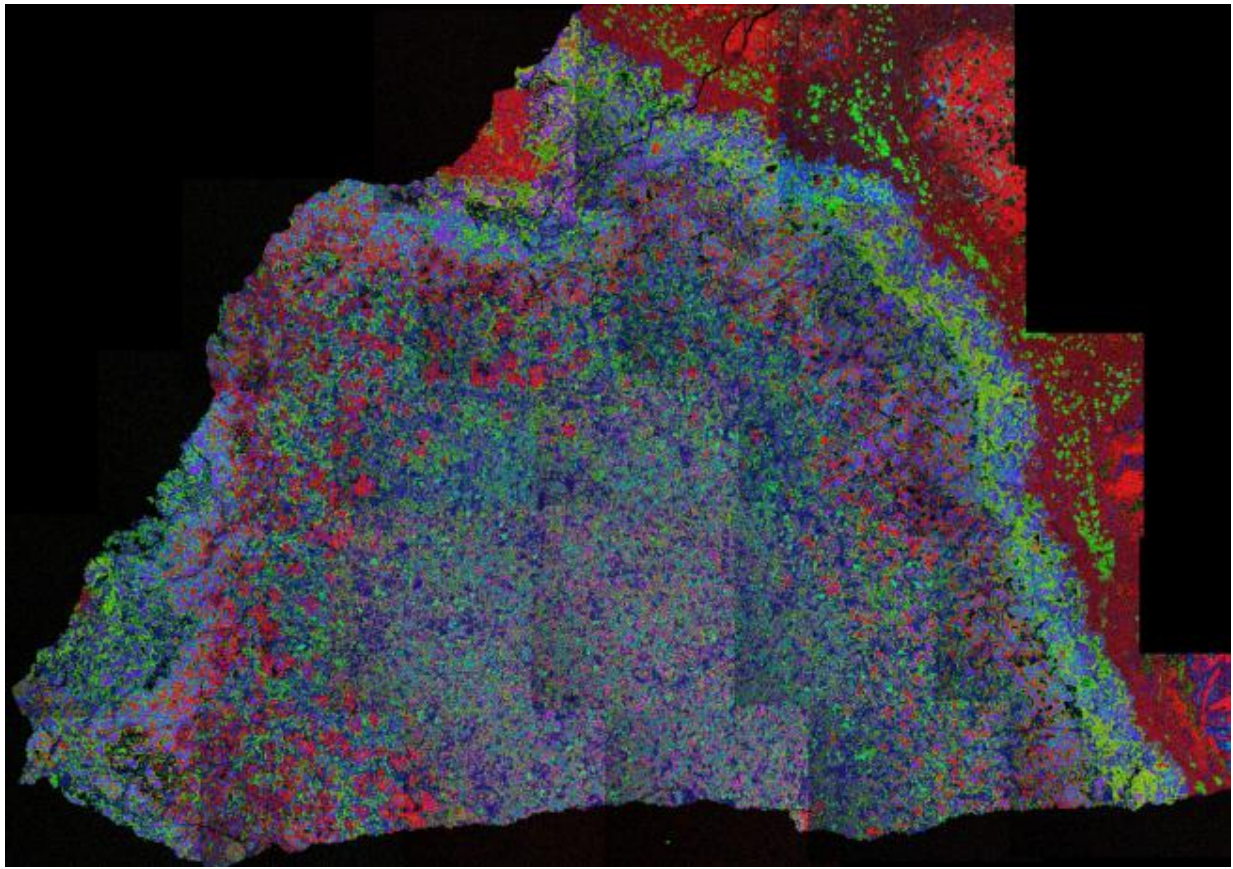


Figure 15: X-ray map of Allende CAI 3507 18B61. Provided by Emma Bullock of the Smithsonian Institute.

Allende 3507 18B61: This is a fine-grained inclusion that has undergone extensive alteration, replacing melilite with secondary minerals such as nepheline, grossular and sodalite (Figure 15). Low-Ti fassaite (<1 wt% TiO₂), olivine and Fe-rich spinel (up to 10 wt%) are present in the core of the inclusion, surrounded by a coarser-grained rim of spinel, fassaite and anorthite. No Wark-Lovering rim is seen enclosing the inclusion.

2.4 Allende Chondrules and Matrix

Chondrules from Allende and Chainpur were also analyzed for HSE abundances and Re-Os systematics. These chondrules were separated by Richard Ash from the

meteorite collection at the University of Maryland. They ranged in mass from ~2 mg to ~9 mg. Rather than processing fragments of chondrules, entire chondrules were analyzed. This was necessary because chondrules have much lower abundances of HSE compared to the highly enriched CAIs (Rubin & Wasson, 1987; Becker *et al.*, 1999). Unfortunately, the necessity to process entire chondrules did not leave enough sample material to make probe mounts for X-ray maps. In the future, larger chondrules will be needed for making both probe mounts and producing trace element data via wet chemistry.

Matrix material was separated from pieces of bulk Allende provided by the Smithsonian Institute. This material was interstitial to all obvious chondrules and CAIs. Samples ranged in mass from ~3 mg to ~28 mg. These samples were processed and analyzed for HSE abundances and Re-Os systematics.

Chapter 3: Methods

3.1 Rare Earth Elements and Classification of Second Suite CAI

The second suite CAIs were analyzed for REE concentrations using the *Thermo-Finnigan Element 2* at the University of Maryland Plasma Mass Spectrometry Lab. Approximately 3 mg of each CAI were separated and crushed into a fine powder. In order to ensure complete digestion, a multiple step digestion sequence was implemented. The CAI separates were initially dissolved in a concentrated 4:1 mixture of HF and HNO₃ at 180°C for two days in a sealed Teflon vessel. After evaporation, the sample residues were then dissolved in 40:10:1 concentrated HF-HNO₃-HClO₄ at 180°C for one day, and then redissolved in HClO₄ two times. The CAI separates were then dried down and redissolved in concentrated HNO₃ three times. They were finally picked up in 0.8N HNO₃ (2 mL) for ICP-MS analysis.

Basaltic standards processed in the same manner contained a white precipitate that became apparent after centrifugation. In order to avoid the production of this precipitate, a different method was used to digest standards. Standards were dissolved in concentrated 4:1 HF:HNO₃ for two days at 180 °C. They were then dried down and picked up in concentrated HCl. After evaporation, the standard residues were dissolved and dried down in concentrated HNO₃ + H₂O₂ several times. They were then redissolved in 0.8N HNO₃. No precipitate was observed using this method. Basaltic standard BCR-2 was used as a reference material to determine concentrations, and basaltic standard BIR-1 was treated as an unknown to determine external reproducibility. BIR-1 was measured periodically along with the CAIs and BCR-2. It was measured in total three times and calculated concentrations among individual BIR-1 measurements varied by less than

$\pm 3\%$. When treated as an unknown, BIR-1 REE data agree with preferred GeoReM BIR-1 values within uncertainty (Figure 16).

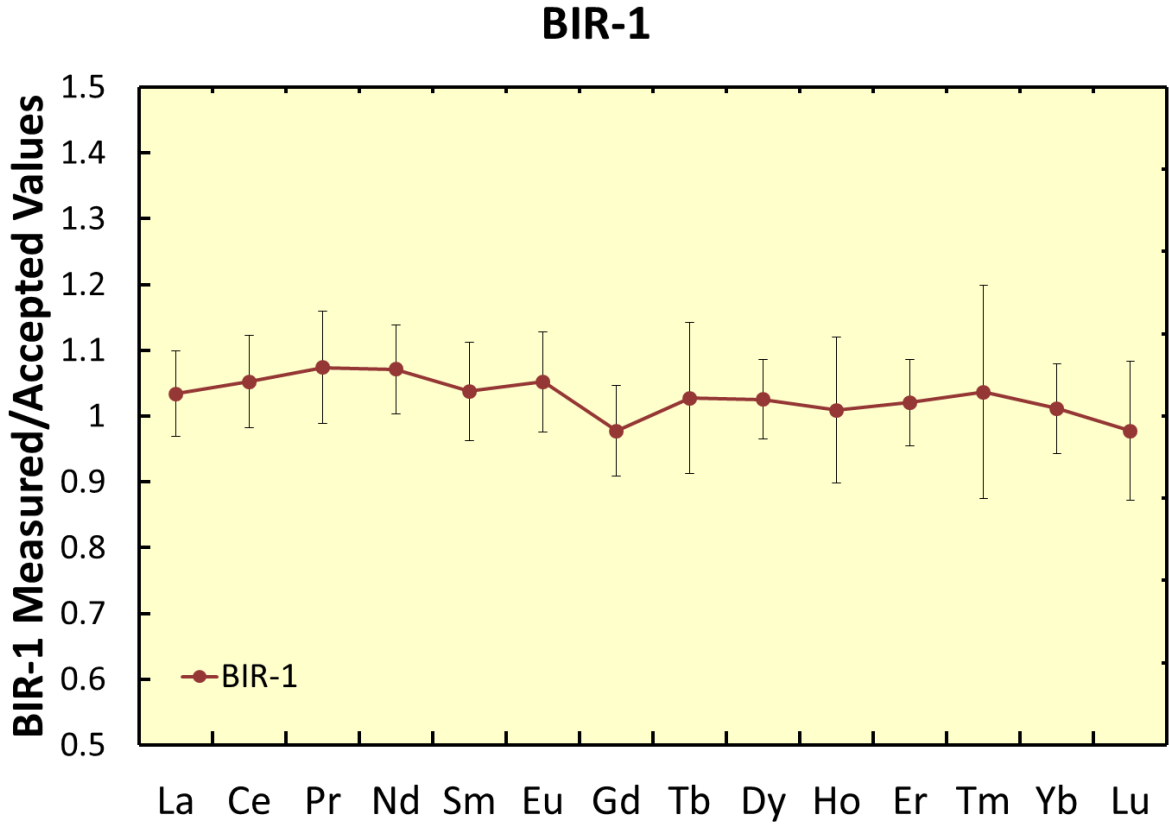


Figure 16: Measured concentrations of BIR-1 from this study compared with GeoReM accepted BIR-1 values. Error bars represent standard deviations of calculated concentrations.

Sample solutions were doped with a 1 ppb In solution in order to assess and correct for instrumental drift. Measurements of isotopes that do not have isobaric interferences, including oxide and argide interferences, were used to determine concentrations. The isotopes measured were La^{139} , Ce^{140} , Pr^{141} , Nd^{146} , Sm^{147} , Eu^{153} , Gd^{157} , Tb^{159} , Dy^{163} , Ho^{165} , Er^{166} , Tm^{169} , Yb^{172} , Lu^{175} and In^{115} .

Signals for samples and standards were corrected for background, blanks, differences among the masses of digested standard and sample materials, differences in degree to which sample or standard solutions were diluted, and instrumental drift using In¹¹⁵ signals. Corrected signals from basaltic standard BCR-2, for which accepted concentrations are well established, were used to determine instrument responses for each of the elements of interest. By comparing the corrected signal, for this standard to each sample, concentrations of the samples were calculated. From these calculated REE abundances, the REE patterns were constructed for classification.

The uncertainties associated with this method stem mainly from signal size variability and the uncertainties reported for accepted BCR-2 standard values. Uncertainties for signal sizes of CAI analyses measured by this study ranged from 3-9%, with a typical uncertainty of around 5%. Reported uncertainties for accepted values were between 0.5% and 7%, with typical uncertainties around 1%. Total uncertainties for calculated concentrations ranged between 5% and around 12%, with typical uncertainties around 7%. Blanks and background signals were less than 0.2% of the signals for standards and samples.

3.2 Highly Siderophile Elements and the Re-Os System in Chondritic Components

For the measurements of HSE and Re-Os systematics, CAI material was carefully scraped from fragments of bulk Allende samples using porcelain tweezers. Contact with lab tools (e.g., steel tweezers) that may have high HSE contents was avoided. In this process, approximately 95-99% pure CAI was removed, with very little contribution from the matrix. Three to five mg of high purity CAI material were then crushed into a fine

powder using an agate mortar and pestle. This material was then combined with isotopic spikes enriched in ^{190}Os , ^{185}Re , ^{99}Ru , ^{194}Pt , ^{191}Ir , and ^{105}Pd . Rhenium and Os were both isotopically enriched using a single mixed spike, and the other four elements were all isotopically enriched using another mixed spike. Spikes, CAIs, and ~3 mL 2:1 teflon distilled concentrated HCl + HNO₃ were combined in 8 mL Pyrex™ Carius tubes (Shirey and Walker, 1995) and heated to 260°C for three days. After digestion, Os was removed from the acid via solvent extraction using CCl₄ and back extraction into HBr (Cohen and Waters, 1996). The Os was then purified by a microdistillation technique from dichromate into HBr (Birck, 1997). All other HSE were purified via chromatography using Bio-Rad columns packed with AG1x8 anion exchange resin.

Purified Os was then analyzed by negative thermal ionization mass spectrometry (N-TIMS) using the UMd VG Sector 54. Before analysis, the Os was dried onto a Pt filament and a Ba(OH)₂ activator was added. Samples were analyzed using either Faraday cup or electron multiplier detectors, depending on the amount of Os separated from the samples. The reported $^{187}\text{Os}/^{188}\text{Os}$ were corrected for instrument bias by measuring a standard at the beginning and end of each session and then correcting sample $^{187}\text{Os}/^{188}\text{Os}$ by comparing the measured standard $^{187}\text{Os}/^{188}\text{Os}$ with an accepted standard $^{187}\text{Os}/^{188}\text{Os}$. For all mass spectrometric sessions, this correction was less than 0.11%.

Rhenium, Ru, Pt, Ir, and Pd were analyzed by MC-ICP-MS on Faraday cup and ion counter detectors using a Nu Plasma multi-collector ICP-MS. Choice of detector depended on the quantities of each element separated. Instrumental biases were corrected by intermittently measuring standards in a standard bracketing technique.

In order to investigate possible cosmic ray interactions with CAIs, Re isotopic compositions were measured via MC-ICP-MS. Samples were prepared in a procedure similar to that used for HSE characterization; however, for these measurements samples were not spiked with enriched isotopes. About 20 mg for group I, III, V, and VI CAIs were used for each analysis in order to achieve sufficiently high precision isotopic measurements. Around ~100 mg of material would be required to analyze any group II CAIs, which was beyond our budget of allocated material. In a method similar to that used for HSE abundance characterization, Re was separated using established anion exchange chromatography methods and measured on the Nu Plasma MC-ICP-MS. Rhenium has only two isotopes, so W was added to the Re-bearing solution in order to correct for mass fractionation. Tungsten has a similar mass range to Re, but no isobaric interferences with ^{185}Re and ^{187}Re .

Chondrules and matrix from Allende were also analyzed for HSE abundances and Re-Os systematics using similar methods previously outlined for CAIs. However, because chondrules have lower HSE concentrations (e.g., lower Re and Os concentrations, Becker *et al.*, 1999) than CAIs and the largest chondrule samples were around ~9 mg, entire chondrules were analyzed rather than fragments. As matrix also has lower concentrations of HSE than CAIs, several larger samples (~15-28 mg) were analyzed.

All HSE and Re-Os analyses were completed over a series of 7 sessions, and a blank was processed for each session. Except for one anomalously high blank, which was not reproduced, blanks for all elements ranged from ~1 to ~17 pg. Averages for each element are as follows: Os, 1.7 ± 1 pg (2σ); Re, 6.0 ± 4.5 pg (2σ); Pd, 15.6 ± 21 pg (2σ);

Pt, 8.9 ± 4.7 pg (2σ); Ru, 17.35 ± 23 pg (2σ); and Ir, 3.8 ± 4.7 pg (2σ). Blank corrections for the Os, Pt, Ru, and Ir abundances of samples were typically less than 0.1%. Palladium corrections ranged from 0.2% to 13%. Rhenium corrections ranged from 0.1% to 7%. Large blank corrections are reflected in the reported uncertainties of the data.

In order to demonstrate analytical accuracy, meteorite in-house standard solutions that have well constrained isotopic compositions were also analyzed on the MC-ICP-MS during several of the spectrometric sessions. This was done for Re, Ir, Ru, and Pt. However, the difficulty in maintaining Pd meteorite standards inhibited the demonstration of external reproducibility. The external reproducibility of meteorite standards for Re, Ir, Ru, and Pt were 2.4%, 1.0%, 1.9%, and 2.3%, respectively. The precision of the reported measurements was determined mostly by the signal intensities and duration of measurements on both N-TIMS and MC-ICP-MS, and is reflected in the 2σ uncertainties listed in the Results section (Tables 2 & 3).

3.3 Nucleosynthetic Anomalies in Trace Elements of CAIs

Osmium isotopic data for unspiked samples were obtained to search for possible isotopic nucleosynthetic heterogeneities in CAIs. For this, samples were prepared in a procedure similar to that for HSE characterization; however, they were not spiked. Prior to anion and cation exchange chromatography, Os was separated via the solvent extraction and HBr back extraction method previously mentioned. They were analyzed via N-TIMS on the *Thermo-Fischer* Triton using Faraday cup collectors. Data were reduced in a method described by Yokoyama *et al.* (2007). Oxide corrections used $^{17}\text{O}/^{16}\text{O}=0.000375$ and $^{18}\text{O}/^{16}\text{O}=0.002044$ (Nier, 1950). All ratios were normalized to

^{189}Os and corrected for mass fractionation using $^{192}\text{Os}/^{189}\text{Os}=2.527411$ (Luck and Allegre, 1983). ^{192}Os and ^{189}Os were used for normalization because they do not have appreciable contributions from s-process nucleosynthesis (Arlandini *et al.*, 1999), and therefore, deviations from solar Os in the form of an s- process enrichment or depletion can be resolved.

Chapter 4: Results

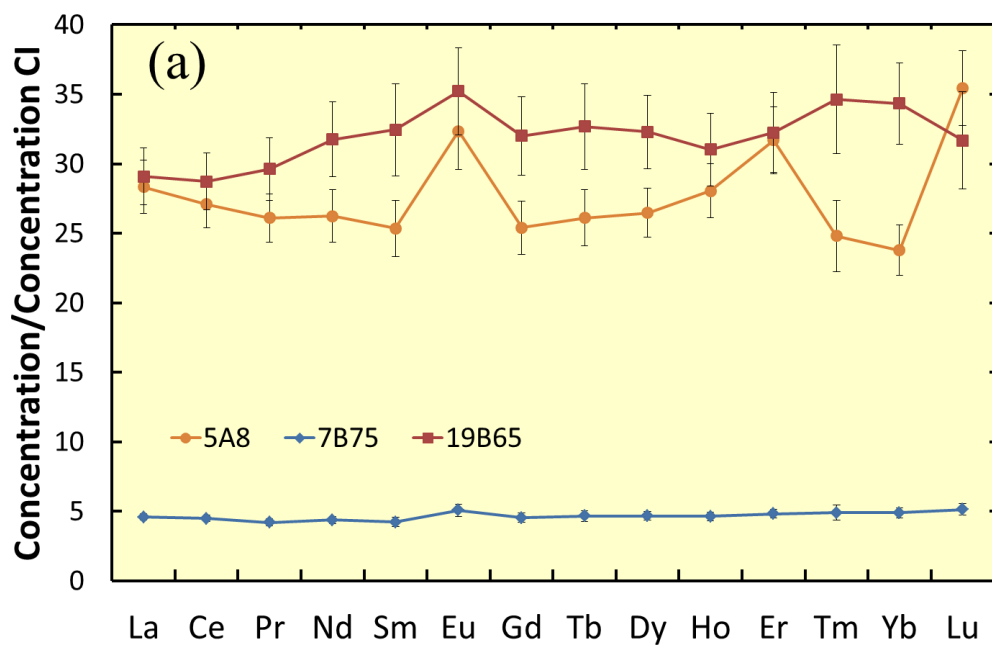
4.1 Classification of Second Suite CAIs

The results of the REE analyses are summarized in Table 1. Based on their REE patterns characterized by positive Eu anomalies, 5A8, 7B75, and 19B65 are classified as belonging to group I CAIs (Figure 17a). CAIs 5A8 and 7B75 have REE abundances about 30x higher than chondritic abundances. Sample 7B75 is characterized by considerably lower abundances of REE of about 5x chondritic (Figure 17b). CAIs 3A7 and 9A30 are characterized by negative Eu and Yb anomalies, which are characteristic of group III CAIs (Figure 17d). These CAIs have abundances 35 times higher than bulk chondritic REE abundances. CAI 18B61 has a highly fractionated REE pattern, with depletions in both the most refractory REE (Gd, Tb, Dy, Ho, Er, Lu), as well as one of the most volatile REE, Yb (17b). This pattern indicates that 18B61 is a group II CAI. The positive Eu anomaly found in 18B61, however, is not consistent with previously reported patterns for group II CAIs (Mason & Taylor, 1982).

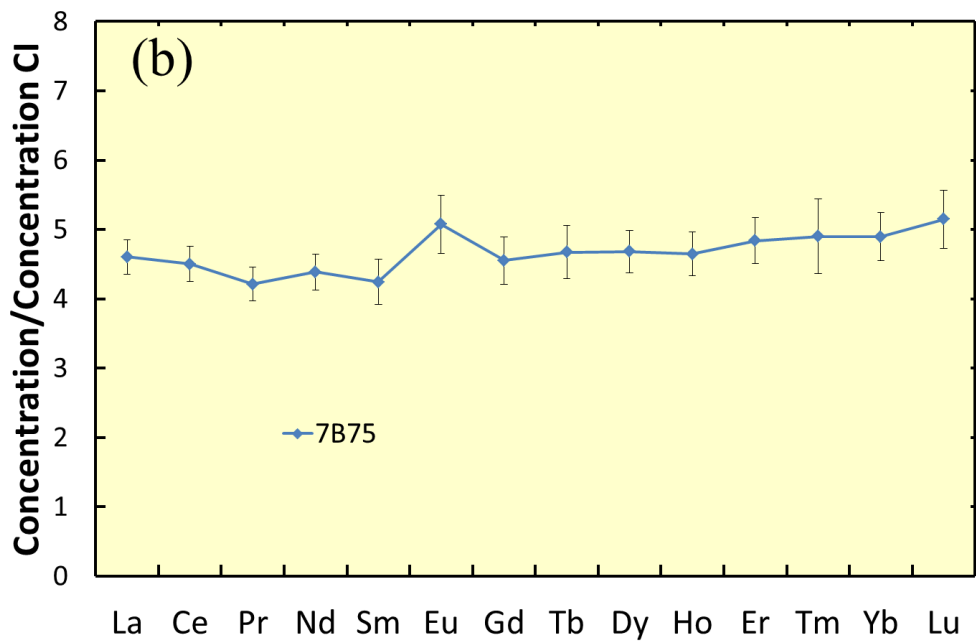
Table 1: Concentrations of REE in Second Suite CAIs in ppm. S.D. in % for concentrations.

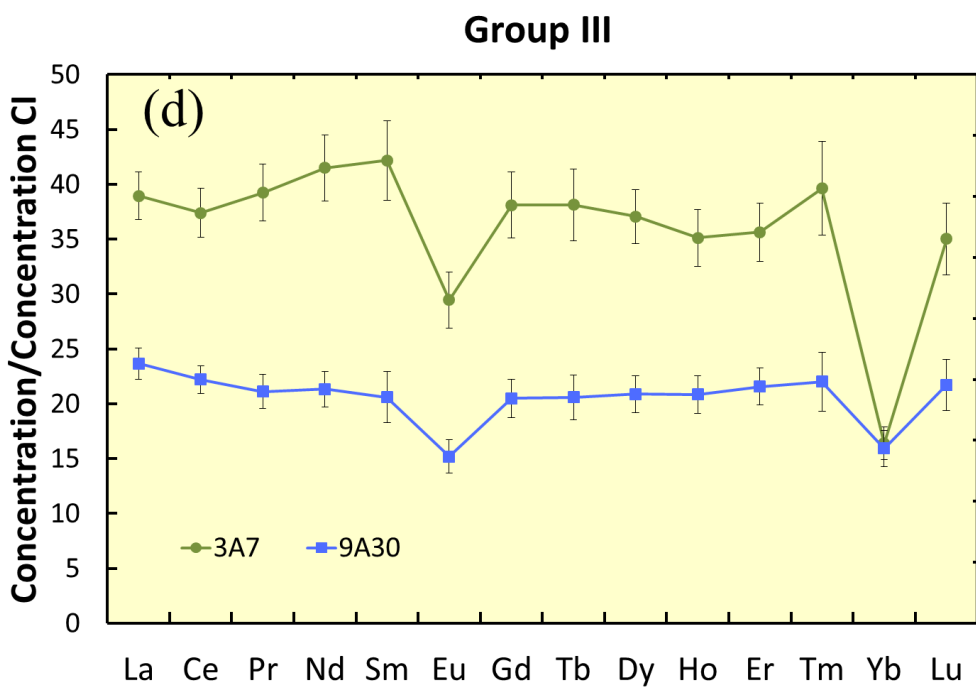
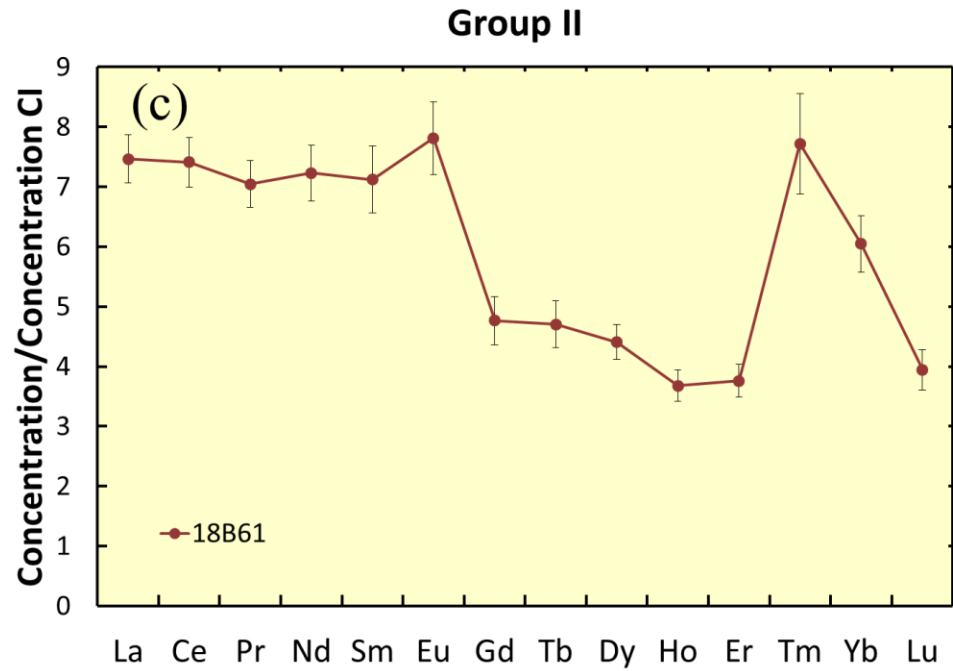
Group	I		I		I		II		III		III	
REE (ppm)	19B65	S.D. [%]	5A8	S.D. [%]	7B75	S.D. [%]	18B61	S.D. [%]	3A7	S.D. [%]	9A30	S.D. [%]
La	6.9	7.0	6.7	6.8	1.1	5.5	1.8	5.3	9.2	5.6	5.1	6.0
Ce	18	7.1	17	6.2	2.8	5.6	4.5	5.6	23	6.0	12	5.5
Pr	2.8	7.7	2.5	6.7	0.40	5.8	0.67	5.6	3.7	6.6	1.8	7.3
Nd	15	8.4	12	7.2	2.0	6.0	3.4	6.4	19	7.3	9.0	7.5
Sm	5.0	10	3.9	8.0	0.65	7.7	1.1	7.8	6.5	8.6	2.8	11
Eu	2.0	8.9	1.9	8.5	0.29	8.3	0.45	7.8	1.7	8.7	0.79	10
Gd	6.6	8.8	5.2	7.5	0.94	7.5	0.98	8.5	7.8	7.9	3.8	8.5
Tb	1.2	9.4	0.98	7.7	0.17	8.2	0.18	8.3	1.4	8.6	0.69	9.9
Dy	8.2	8.2	6.7	6.7	1.2	6.6	1.1	6.6	9.4	6.7	4.8	8.1
Ho	1.8	8.5	1.6	7.0	0.26	6.9	0.21	7.1	2.0	7.3	1.1	8.2
Er	5.3	8.9	5.2	7.6	0.80	6.9	0.62	7.4	5.9	7.5	3.2	7.8
Tm	0.88	11	0.63	10	0.13	11	0.20	11	1.0	11	0.51	12
Yb	5.8	8.6	4.0	7.7	0.83	7.1	1.0	7.8	2.8	8.9	2.4	10
Lu	0.80	11	0.90	7.6	0.13	8.2	0.10	8.7	0.89	9.3	0.50	11

Group I



Group I (7B75)





Figures 17(a-d): Chondrite-normalized REE patterns of 6 Allende CAIs: (a) group I CAIs (b) group I CAI 7B75 with smaller scale, (c) group II CAIs (d) group III CAIs.

4.2 Highly Siderophile Elements in Chondritic Components

4.2.1 Highly Siderophile Elements in Calcium-Aluminum-Rich Inclusions

The results for HSE abundances of CAIs, chondrules, and matrix are summarized in Table 2. Highly siderophile element abundances normalized to Orgueil, a CI1 chondrite, are shown in Figures 18 and 19 for the first and second suite CAIs analyzed by this study. Because group II CAIs and non-group II CAIs have distinctly different HSE abundance patterns, they will be discussed separately. Non-group II CAI 5A8 has anomalous HSE abundances in reference to the other non-group II CAIs and will also be discussed separately from the other non-group II CAIs.

The CI1 chondrite normalized-patterns for Allende CAIs (Figures 18 & 19) are generally consistent with previously reported patterns (Figure 3), except for consistently lower concentrations of Pd for non-group II CAIs than those measured by spark source mass spectrometry (SSMS) and reported by Mason & Taylor (1982). A comparison of Os/Pd for all group I and III CAIs analyzed in this study and Mason & Taylor (1982) indicate higher ratios for the new data (Figure 20). However, a comparison of other HSE (e.g., Os/Pt) between the two studies agree well (Figure 21).

Osmium concentrations of most CAIs defined as non-group II CAIs range from 210.4 ppb to 1044 ppb. Rhenium abundances vary from 2714 to 12700 ppb for these same CAIs. Abundances of Ir, Ru, Pt, and Pd range from 2570 to 17860 ppb, 4221 to 24600 ppb, 4541 to 40690 ppb, and 35.40 to 354.5 ppb, respectively. Within the suite of non-group II CAIs analyzed by this study, concentrations of HSE vary by factors of ~5 to 9. Osmium has the lowest degree of variation, varying only by a factor of 4.7. Platinum has the highest degree of variation, varying by a factor of 9.0.

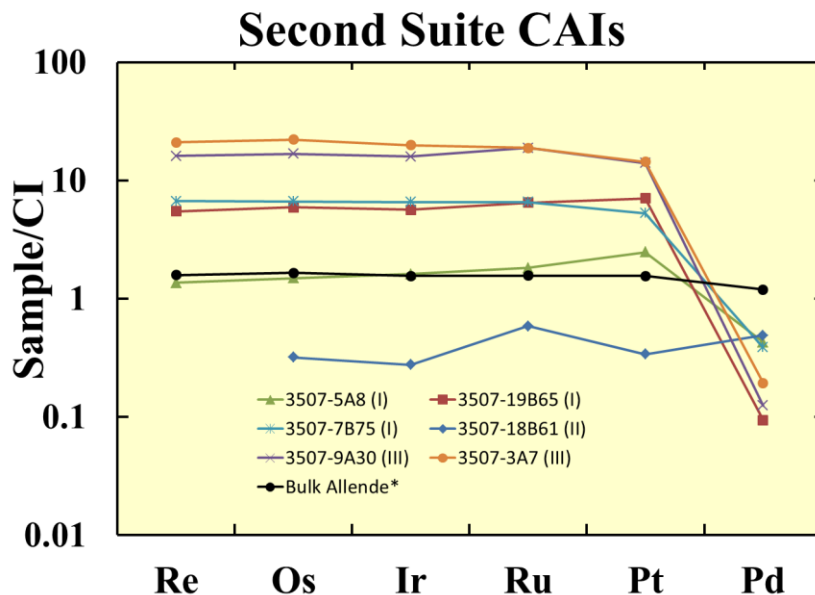
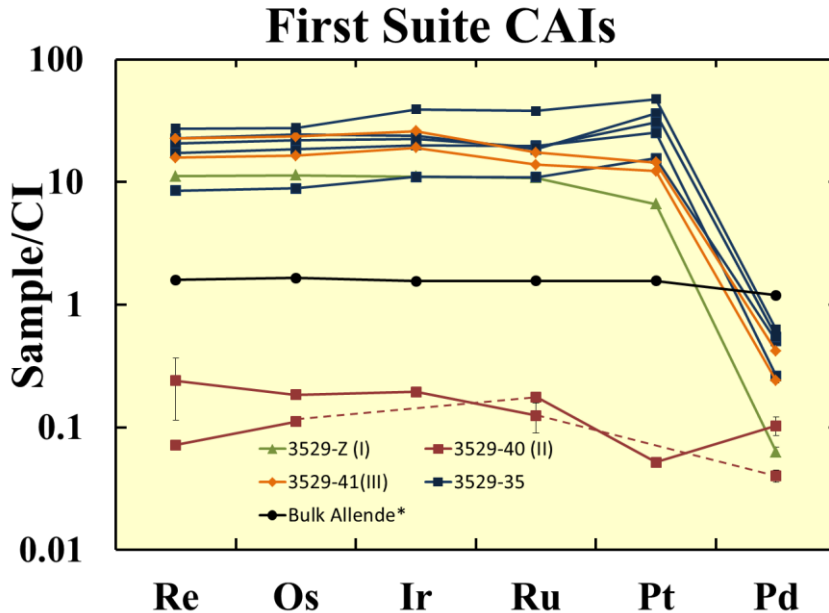
CAI 3529-40, previously classified as a group II CAI, is characterized by a subchondritic HSE pattern, and is consistent with HSE patterns of other group II CAIs (Mason & Taylor, 1982). This group II CAI also does not have a negative Pd anomaly, which is also consistent with previously reported HSE abundances of group II CAIs. The low concentrations of HSE in group II CAIs coupled with the small sample size for 3529-40 yielded signals too small for analyses of Ir in one analysis of 3529-40 and Pt for another analysis of this CAI. Analyses of larger sample sizes of group II CAIs are needed to produce complete abundance patterns.

Despite being classified as a group I CAI, 5A8 has lower absolute abundances of HSE than other group I CAIs, and a pattern unlike any non-group II CAIs analyzed by this study. It does, however, have a large Pd depletion relative to the other HSE, consistent with non-group II CAIs.

Replicate HSE analyses of the same CAIs have reproducible pattern shapes; however, absolute abundances vary. For example, 5 separate analyses of CAI 3529-35 have HSE abundances that vary by as much as a factor of 3.6 for any single element. Variances of absolute HSE abundances within separate analyses of the same CAIs have been reported in other studies (Becker *et al.*, 2001; Mason & Taylor, 1982).

Table 2: Highly siderophile element concentrations of a suite of CAIs separated in the 1970s ("First Suite CAIs"), and a suite of recently separated CAIs ("Second Suite CAIs"), chondrules, and matrix. All samples were taken from Allende, except for Chainpur A and B. ^a-Average bulk Allende calculated from several bulk Allende analyses from Horan *et al.* (2003) and Walker *et al.* (2002).

	CAI Group	Weight (mg)	Re (ppb)	Os (ppb)	Ir (ppb)	Ru (ppb)	Pt (ppb)	Pd (ppb)
First Suite CAIs								
3529-Z	I	3.93	427.9	5199	5063	7044	5685	35.40
3529-40	II	3.34	9.204	84.60	88.69	80.87	n.d.	22.65
Replicate	II	2.02	2.756	50.94	n.d.	114.6	44.76	58.15
3529-41	III	3.64	869.4	1079	11870	11280	12410	235.4
Replicate	III	2.51	603.8	7496	8652	8988	10570	134.9
3529-35		3.88	1044	12700	17860	24600	40690	354.5
Replicate		3.10	325.6	4082	5015	7106	13440	284.2
Replicate		2.04	660.4	8524	9074	12830	21650	148.4
Replicate		2.52	866.0	11160	10880	12010	31140	308.4
Replicate		4.19	794.9	10040	10190	12460	26510	n.d.
Second Suite CAIs								
3507-5A8	I	3.67	52.37	684.8	735.9	1183	2126	241.6
3507-7B75	I	1.27	255.9	3047	2989	4275	4541	218.1
3507-19B65	I	6.31	210.4	2714	2569	4221	6081	53.05
3507-18B61	II	1.89	n.d.	146.8	126.2	380.6	292.4	276.6
3507-9A30	III	2.56	617.1	7687	7245	12220	12070	70.13
3507-3A7	III	3.53	805.8	10150	9070	12210	12330	109.3
Chondrules								
Allende A		8.90	4.576	58.36	58.17	92.16	131.7	160.1
Allende B		5.94	75.80	965.9	946.8	1078	2274	204.2
Allende C		4.63	32.58	383.6	374.1	423.7	510.8	75.81
Allende D		3.37	17.95	238.6	193.1	300.2	397.7	230.4
Allende E		6.78	84.67	1198	1397	1479	2837	617.5
Allende F		2.20	111.2	1270	1433	1413	1900	5.303
Chainpur A		3.20	35.71	428.0	431.5	505.3	675.3	20.2
Chainpur B		4.22	57.18	646.1	648.4	806.8	1100	163
Matrix								
Matrix 1		3.53	48.58	647.6	592.3	922.1	1330	1067
Matrix 2		3.64	42.69	575.4	569.2	800.5	1447	1059
Matrix 3		13.97	136.5	911.9	861.6	890.4	1100	633.6
Matrix 4		10.39	45.62	614.5	638.0	766.1	1139	591.0
Bulk Allende^a			60.94	758.0	710.4	1016	1341	671.9



Figures 18 and 19: Abundance patterns of HSE in Allende CAIs normalized to CI chondrite concentrations. Roman numerals represent group classification based on REE abundances. Replicate analyses for the same CAI are represented by the same symbols and line colors. Dashed lines represent lack of data. First suite CAIs were separated in the 1970s. Second suite CAIs were recently separated. Bulk Allende^a averaged from multiple bulk Allende analyses from Horan *et al.* (2003) and Walker *et al.* (2002).

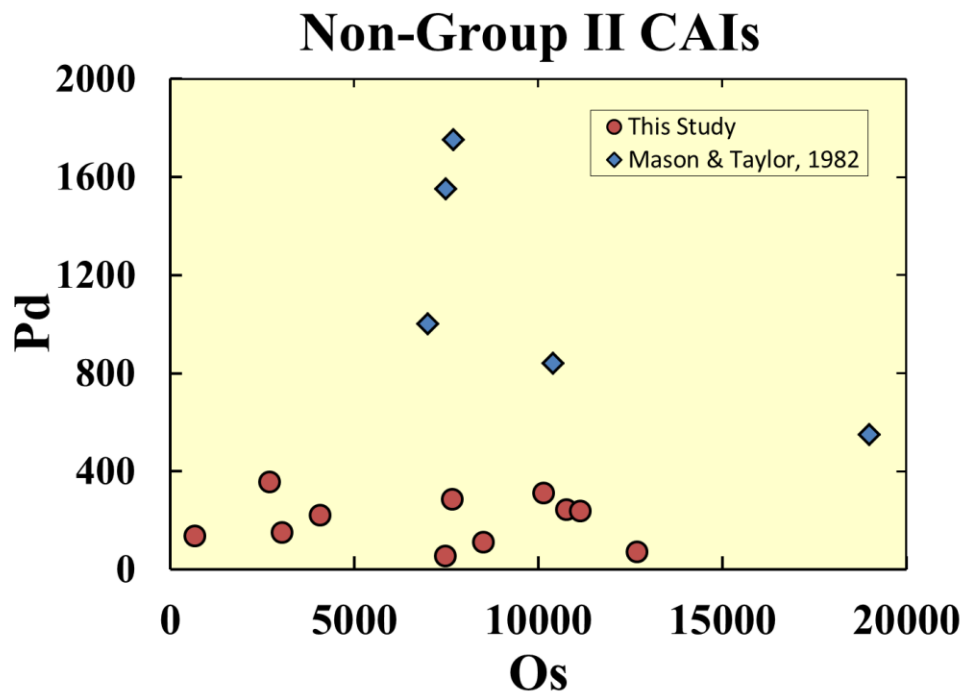


Figure 20: Pd vs. Os abundances, in ppb, of Allende non-group group II CAIs. “Mason & Taylor, 1982” refers to data taken directly from that study.

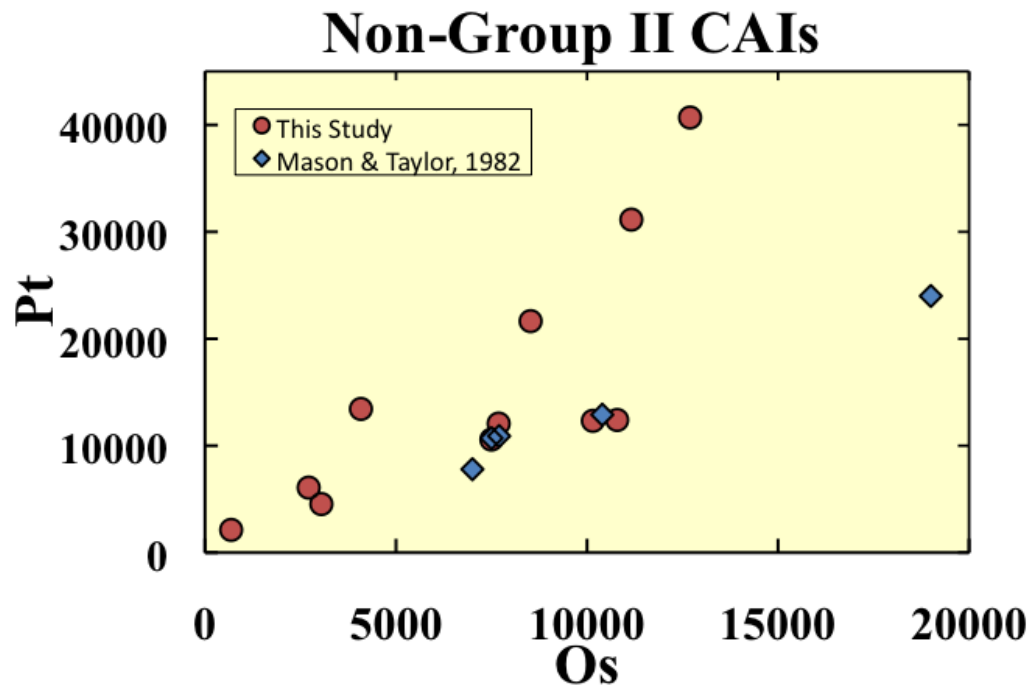


Figure 21: Pt vs. Os abundances, in ppb, of Allende non-group II CAIs. “Mason & Taylor, 1982” refers to data taken directly from that study.

4.2.2 Highly Siderophile Elements in Chondrules

HSE abundances of Allende and Chainpur chondrules are provided in Table 2. CI1 chondrite-normalized HSE patterns are shown in Figure 22. Chondrules from Allende and the ordinary chondrite Chainpur show similar HSE patterns. Comparing Re, Os, Ir, Ru, Pt, and Pd abundance patterns of bulk Allende and Chainpur chondrules from this study with previous studies is not possible, as analyses of the entire set of elements examined in this study have not been published before. Prior studies have reported Re, Os, and Ir data for bulk chondrules. Our new data are in good agreement with these data (e.g., data from Rubin & Wasson, 1987; Becker *et al.*, 1999, Walker *et al.*, 2002) (Figure 22). Due to the small sample sizes of this suite of chondrules and lower concentrations of HSE in chondrules, entire chondrules were processed for abundance data. Without multiple fractions of the same chondrules, replicate analyses of individual chondrules were not conducted.

Three CAIs have suprachondritic refractory HSE abundances, whereas three other CAIs have subchondritic refractory HSE abundances. Rhenium and Os concentrations define a range of 4.58 to 111.2 and 58.361 to 1270 ppb, respectively, for 8 chondrules. These correspond to ranges that vary by factors of ~24 and ~22, respectively. Iridium, Ru, Pt, and Pd, concentrations range from 58.17 to 1397, 92.16 to 1684, 131.7 to 2837, and 5.303 to 617.5 ppb, respectively. Iridium, Ru, and Pt, vary by factors of ~25, ~16, and ~21.5, respectively. Palladium shows the greatest amount of variation, varying by a factor of ~116. Like CAIs, with the exception of chondrule F, all chondrules show negative Pd anomalies relative to the other HSE (Figure 22).

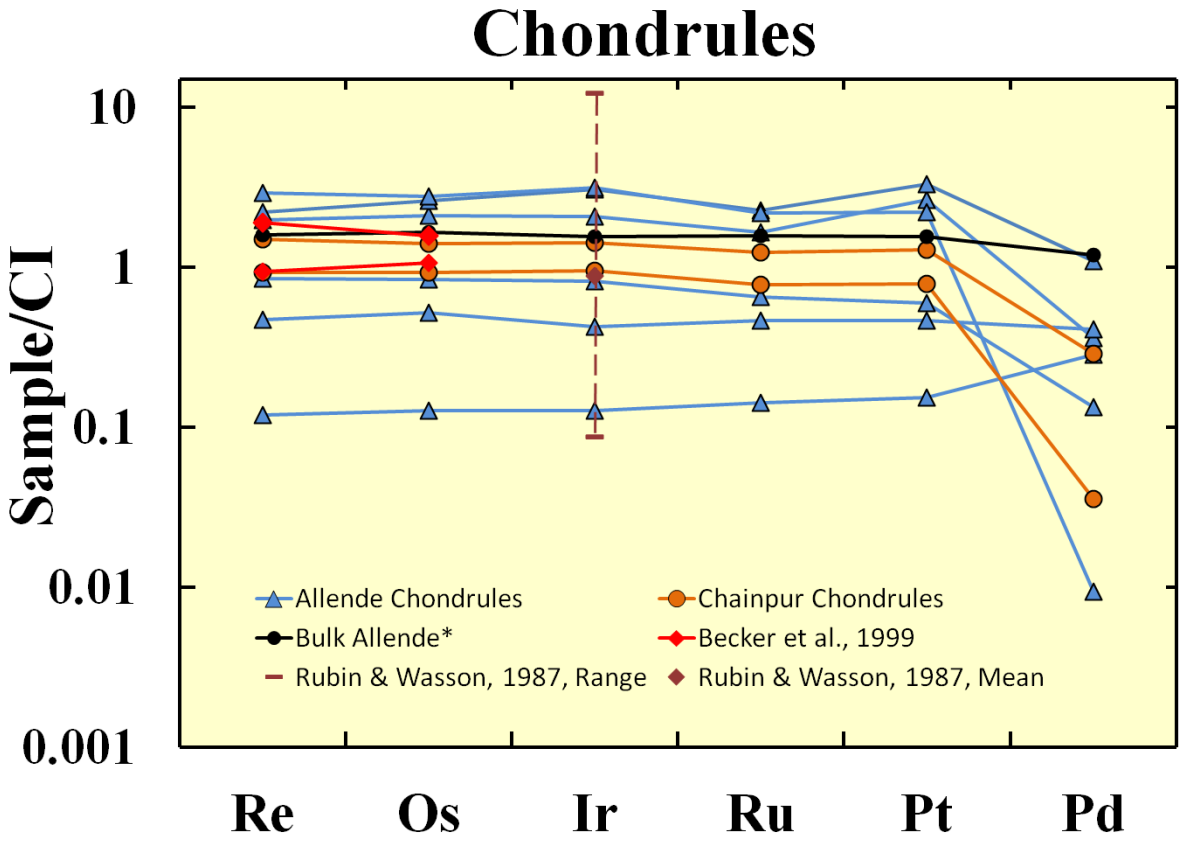


Figure 22: Abundance patterns of HSE in Allende and Chainpur chondrules normalized to CI chondrite concentrations. All chondrules were separated by R.D. Ash at the University of Maryland. Bulk Allende^a averaged from multiple bulk Allende analyses from Horan *et al.* (2003) and Walker *et al.* (2002).

4.2.3 Highly Siderophile Elements in Matrix

Data for matrix material are reported in Table 2. CI1 chondrite-normalized HSE patterns for matrix are shown in Figure 23. Matrix shows the least amount of HSE variation for Allende components analyzed by this study. Rhenium and Os abundances vary only from 42.69 to 136.5 and 575.4 to 911.9, respectively. The other HSE show little variation as well, with Ir, Ru, Pt, and Pd varying by 569.2 to 861.6, 766.1 to 922.1, 1100 to 1447, and 591 to 1067 ppb, respectively. All HSE, except for Re, vary by a

factor of less than 2. Rhenium varies by a factor of ~3. The two chondrite-normalized matrix patterns closely resemble bulk Allende. However, matrix 1 and matrix 2 have slight enrichments in Pd, and matrix 3 has a slight enrichment in Re.

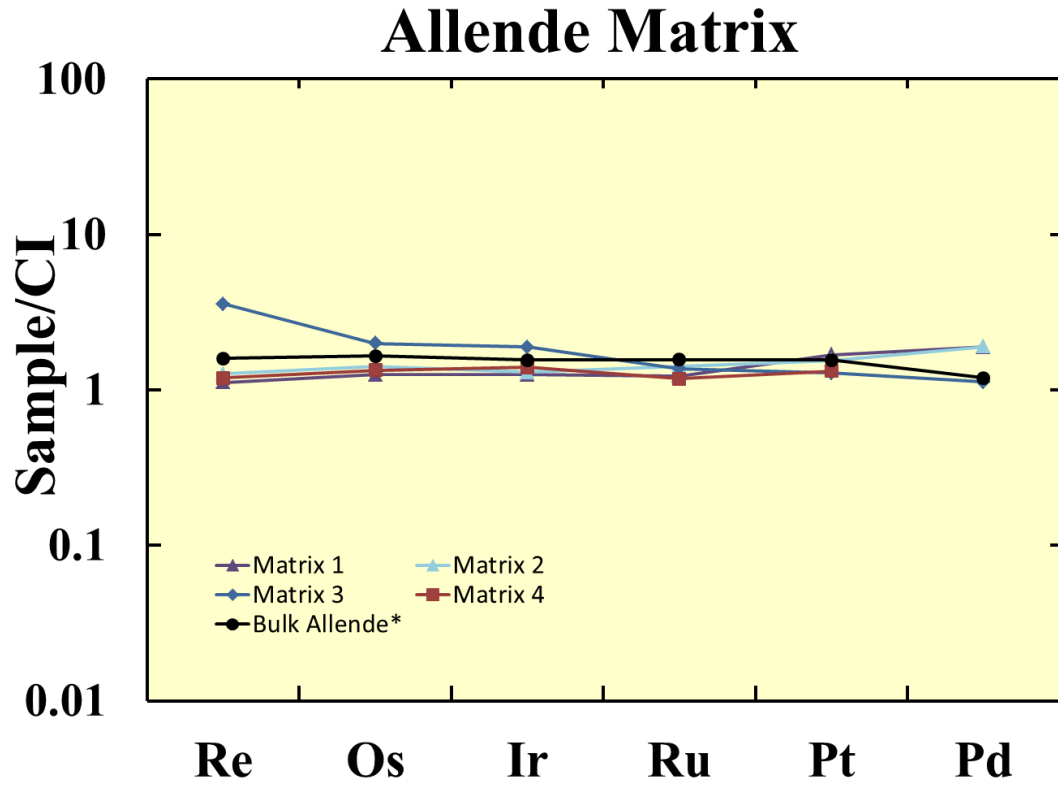


Figure 23: Abundance patterns of HSE in Allende matrix normalized to CI chondrite concentrations. Bulk Allende^a averaged from multiple bulk Allende analyses from Horan *et al.* (2003) and Walker *et al.* (2002).

4.3 Rhenium-Osmium Systematics of Allende Components

Results for the Re-Os system of Allende CAIs, chondrules, and matrix are provided in Table 3. Group II CAIs and non-group II CAIs are discussed separately because their Re-Os systematics are very different. For the non-group II CAIs in both suites, $^{187}\text{Re}/^{188}\text{Os}$ ranges from 0.3684 to 0.4047, and $^{187}\text{Os}/^{188}\text{Os}$ ranges from 0.12588 to 0.12874. The range of $^{187}\text{Re}/^{188}\text{Os}$ falls within the range defined by Allende and other

carbonaceous chondrites (Walker *et al.*, 2002; Fischer-Gödde *et al.*, 2010). However, the upper end of the range of $^{187}\text{Os}/^{188}\text{Os}$ for the CAIs analyzed by this study is above the range defined by the carbonaceous chondrites analyzed in Walker *et al.* (2002).

Only one group II CAI, 3529-40, was successfully analyzed for Re-Os systematics. With a $^{187}\text{Re}/^{188}\text{Os}$ of 0.5240, 3529-40 falls outside of the range defined by the non-group II CAIs. However, the $^{187}\text{Os}/^{188}\text{Os}$ of 3529-40 is 0.12774, which falls within the range of non-group II CAI data. This CAI plots beyond analytical uncertainty of the primordial reference isochron.

The total absolute deviations of both $^{187}\text{Re}/^{188}\text{Os}$ and $^{187}\text{Os}/^{188}\text{Os}$ from a primordial 4558 Myr isochron, multiplied by 10^4 , is defined using the Δ_{Os} notation (Becker *et al.*, 2001; Walker *et al.*, 2002):

$$\Delta_{\text{Os}} = 10^4 ({}^{187}\text{Os}/{}^{188}\text{Os}_{\text{CAI}} - (0.09524 + 0.07887 {}^{187}\text{Re}/{}^{188}\text{Os}_{\text{CAI}})) \quad (\text{Eqn. 1})$$

where ${}^{187}\text{Os}/{}^{188}\text{Os}_{\text{CAI}}$ and ${}^{187}\text{Re}/{}^{188}\text{Os}_{\text{CAI}}$ are the measured isotopic compositions of a given sample, and 0.09524 and 0.07887 are the initial ${}^{187}\text{Os}/{}^{188}\text{Os}$ and slope of the IIIA iron meteorite isochron, respectively (Smoliar *et al.*, 1996).

Assuming CAIs formed from a reservoir with a uniform ${}^{187}\text{Os}/{}^{188}\text{Os}$ isotopic composition within ~ 20 Myr of the beginning of the Solar System, CAIs should plot on a primordial isochron if the system remained closed from CAI formation until today (Smoliar *et al.*, 1996). The Re-Os isochron and Δ_{Os} plot (Figures 24, 25, & 26) show that while 6 out of 14 analyses of CAIs plot within ± 5 Δ_{Os} units of a primordial Re-Os isochron, only one plots on the primordial Re-Os isochron within analytical uncertainty.

The majority of the CAI analyses (8 out of 14) in this study plot beyond uncertainties of a primordial isochron by more than $\pm 5 \Delta_{\text{Os}}$ units.

Within the Allende chondrules analyzed here, more variability is seen in both $^{187}\text{Re}/^{188}\text{Os}$ and $^{187}\text{Os}/^{188}\text{Os}$ than in non-group II CAIs. The $^{187}\text{Re}/^{188}\text{Os}$ and $^{187}\text{Os}/^{188}\text{Os}$ of the six chondrules analyzed range from 0.3405 to 0.4221 and 0.12449 to 0.12854, respectively (Table 3). These values reflect variations of $\sim 24\%$ and $\sim 3\%$, respectively. In contrast, the CAIs analyzed here show variations on the order of $\sim 10\%$ and $\sim 2\%$ for $^{187}\text{Re}/^{188}\text{Os}$ and $^{187}\text{Os}/^{188}\text{Os}$. The Re-Os systematics of Chainpur chondrules fall within the ranges defined by Allende CAIs.

The Re-Os isochron for 6 Allende chondrules (Figure 26) shows that some, but not all, of these Allende components also plot off of a primordial IIIA iron meteorite isochron. Allende chondrule A plots near the primordial isochron with a Δ_{Os} of 26.8 ± 23.0 (2σ). However, all 5 other chondrules plot off the primordial isochron within uncertainty.

Three out of four Allende matrix samples analyzed have a much tighter range of $^{187}\text{Re}/^{188}\text{Os}$ and $^{187}\text{Os}/^{188}\text{Os}$ compared to both CAIs and chondrules. Excluding matrix 3, the range in $^{187}\text{Re}/^{188}\text{Os}$ and $^{187}\text{Os}/^{188}\text{Os}$ for matrix is 0.3573 to 0.3614 ($\sim 1\%$ variation) and 0.12483 to 0.12574 ($\sim 0.6\%$ variation), respectively. Matrix 3 has an extremely high $^{187}\text{Re}/^{188}\text{Os}$ of 0.7213, but a normal $^{187}\text{Os}/^{188}\text{Os}$ of 0.12679.

Becker *et al.* (2001) reported that Re-Os data from CAI 3529-41 formed a linear array on an isochron diagram defining an age of 1614 ± 39 Myr. Six of the Allende CAIs analyzed by this study plot within analytical uncertainty of the same isochron. Also, three Allende chondrules, B, E, and F, plot on or close to the CAI internal isochron from

Becker *et al.* (2001). Allende matrix also shows deviations from a primordial isochron, with one datum plotting on the CAI internal isochron (1614 ± 39 Myr), and one datum point plotting on the primordial isochron within uncertainty.

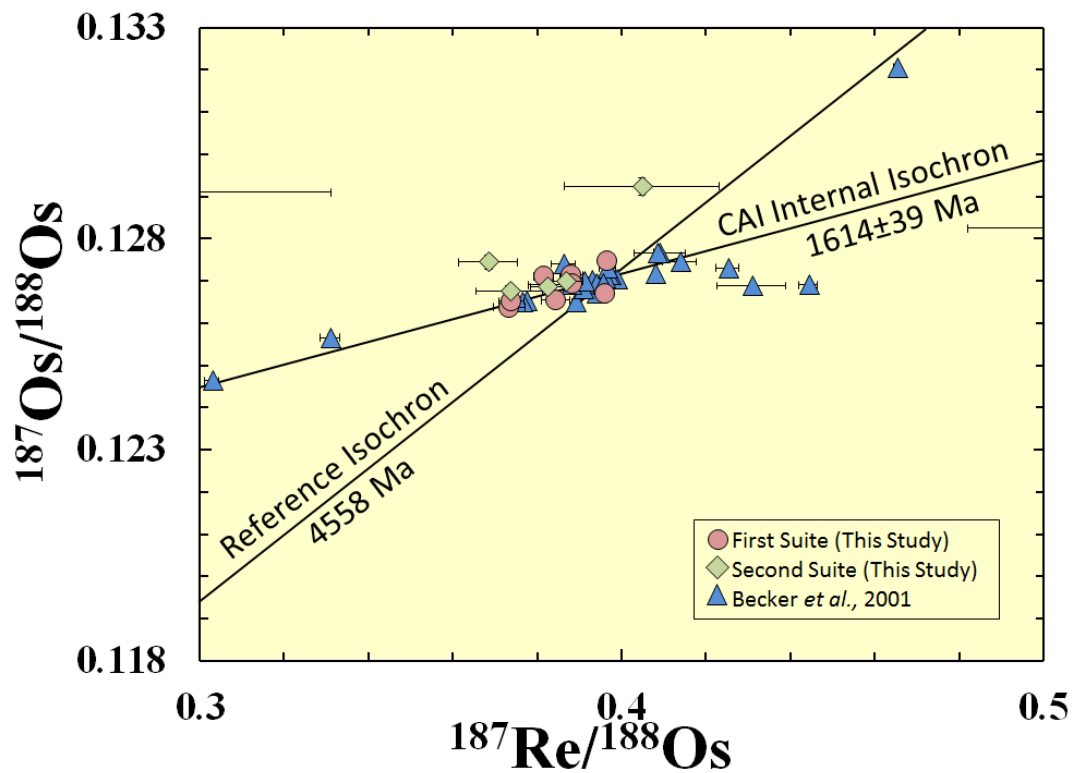
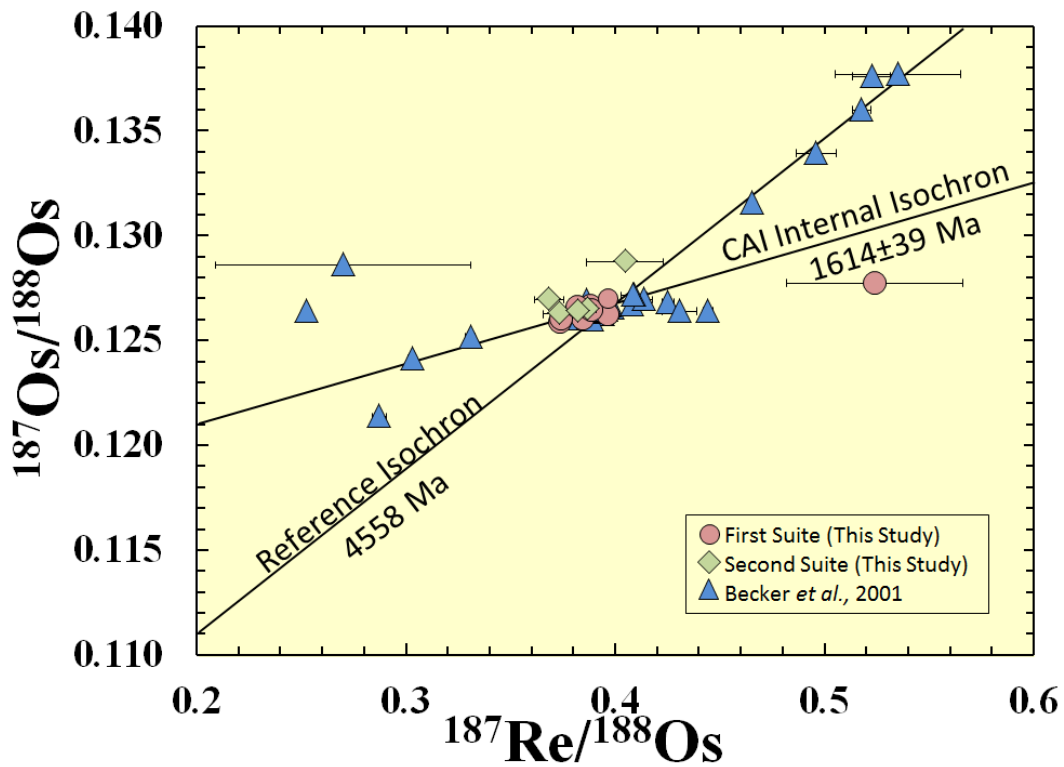
4.4 Rhenium and Osmium Isotopic Compositions

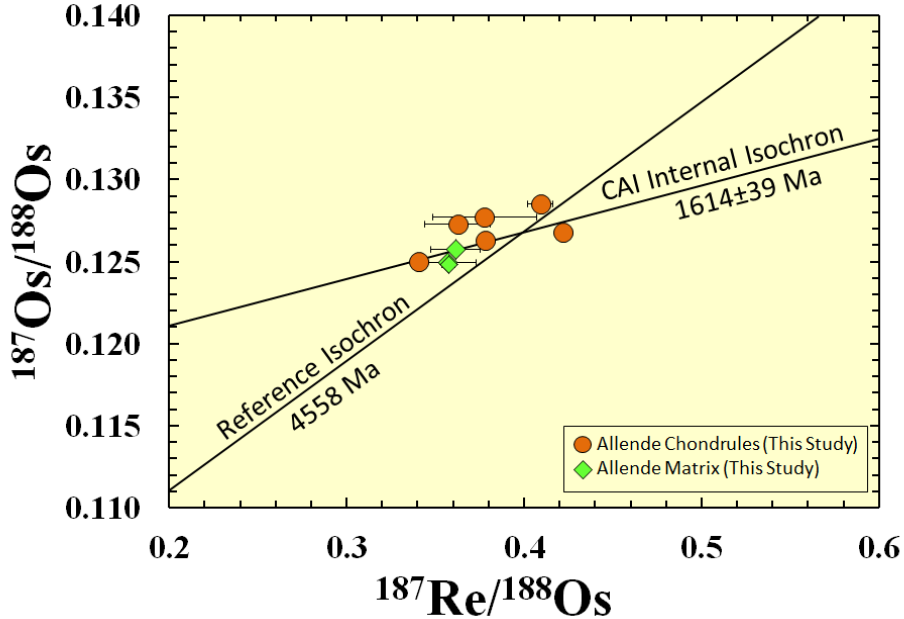
Two unspiked CAIs were measured for the isotopic composition of Re in order to determine if cosmic ray interactions altered the Re isotopic composition of CAIs and caused apparent non-isochronous behavior. The Re isotopic compositions measured for these CAIs were 0.60070 ± 0.0001 (2σ) and 0.60043 ± 0.00009 (2σ), for CAIs 3529-35 and 3507-19B65, respectively. Compared to a terrestrial standard with a Re isotopic composition of 0.59817 ± 0.00017 (2σ), the Re isotopic composition of these CAIs appears to be resolvably higher than that of the terrestrial standard.

Two unspiked Allende CAIs were also measured for the isotopic composition of Os in order to examine possible nucleosynthetic anomalies in CAIs (Table 4; Figure 28). The Os isotopic compositions of these CAIs cannot be distinguished from the terrestrial standard within uncertainty.

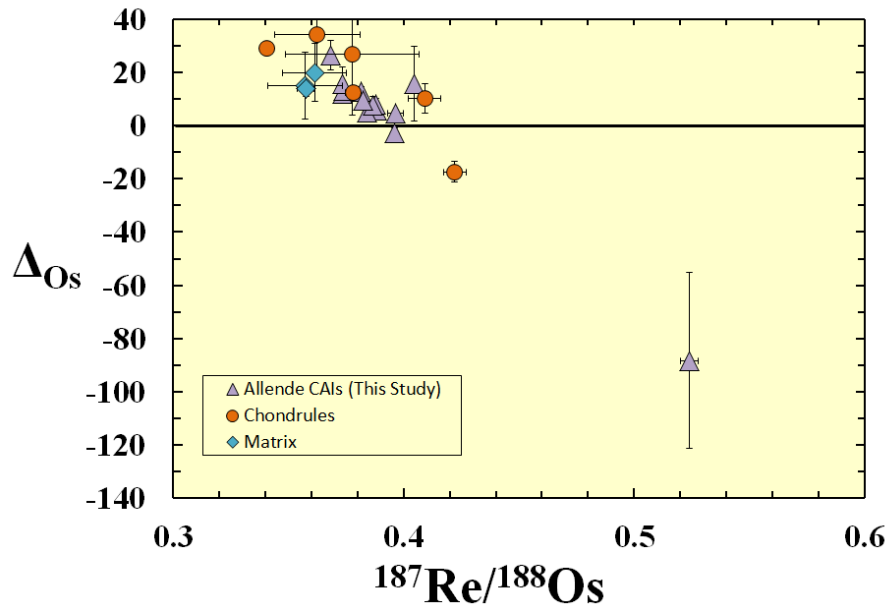
Table 3: Re-Os systematics of a suite of CAIs separated in the 1970s ("First Suite CAIs"), and a suite of recently separated CAIs ("Second Suite CAIs"), chondrules, and matrix. All samples were taken from Allende, except for Chainpur A and B. Uncertainties of $^{187}\text{Re}/^{188}\text{Os}$ and $^{187}\text{Os}/^{188}\text{Os}$ are 2σ and include external precision and uncertainty based on Re blanks.

	CAI Group	Weight (mg)	$^{187}\text{Re}/^{188}\text{Os}$	2σ	$^{187}\text{Os}/^{188}\text{Os}$	2σ	ΔOs	2σ
First Suite CAIs								
3529-Z	I	3.93	0.3965	0.0010	0.12697	0.00015	4.6	0.8
3529-40	II	3.34	0.5240	0.0420	0.12774	0.00027	-88.3	33.1
Replicate	II	2.02	n.d.		n.d.			
3529-41	III	3.64	0.3882	0.0022	0.12644	0.00014	5.8	1.7
Replicate	III	2.51	0.3880	0.0027	0.12664	0.00026	8.0	2.1
3529-35		3.88	0.3959	0.0021	0.12621	0.00016	-2.6	1.7
Replicate		3.10	0.3843	0.0034	0.12604	0.00016	5.0	2.7
Replicate		2.04	0.3733	0.0038	0.12588	0.00016	12.0	3.0
Replicate		2.52	0.3738	0.0029	0.12603	0.00010	13.1	2.3
Replicate		4.19	0.3815	0.0024	0.12661	0.00008	12.8	1.9
Second Suite CAIs								
3507-5A8	I	3.67	0.3684	0.0070	0.12694	0.00016	26.5	5.5
3507-7B75	I	1.27	0.4047	0.0180	0.12874	0.00020	15.8	14.2
3507-19B65	I	6.31	0.3734	0.0079	0.12626	0.00011	15.7	6.2
3507-18B61	II	1.89	n.d.		n.d.			
3507-9A30	III	2.56	0.3867	0.0041	0.12650	0.00010	7.6	3.2
3507-3A7	III	3.53	0.3823	0.0038	0.12635	0.00007	9.6	3.0
Chondrules								
Allende A		8.90	0.3778	0.0292	0.12771	0.00026	26.8	23.0
Allende B		5.94	0.3781	0.0031	0.12630	0.00017	12.4	2.5
Allende C		4.63	0.4092	0.0071	0.12854	0.00018	10.2	5.6
Allende D		3.37	0.3625	0.0186	0.12726	0.00017	34.3	14.7
Allende E		6.78	0.3405	0.0023	0.12499	0.00016	29.0	1.9
Allende F		2.20	0.4221	0.0049	0.12680	0.00017	-17.3	3.9
Chainpur A		3.20	0.4020	0.0090	0.12851	0.00018	15.7	7.1
Chainpur B		4.22	0.4265	0.0049	0.12787	0.00050	-10.1	3.9
Matrix								
Matrix 1		3.53	0.3614	0.0140	0.12574	0.00016	20.0	11.0
Matrix 2		3.64	0.3573	0.0160	0.12491	0.00018	14.9	12.6
Matrix 3		13.97	0.7213	0.0035	0.12679	0.00014	-253.4	2.8
Matrix 4		10.39	0.3575	0.0037	0.12483	0.00010	13.9	2.9





Figures 24, 25, and 26: (First Figure) Re-Os systematics of Allende CAIs. Data is also included from Becker *et al.* (2001). (Second Figure) Re-Os systematics of Allende CAIs with a smaller scale. (Third Figure) Re-Os systematics of chondrules and Allende matrix. Reference isochron is for a IIIA iron meteorite (Smoliar *et al.*, 1996). Error bars are either shown or are smaller than the symbol.



Figures 27: Δ_{Os} vs. $^{187}\text{Re}/^{188}\text{Os}$ of Allende CAIs, chondrules, and matrix. Δ_{Os} is a measure of the absolute deviation of a sample from a IIIA iron meteorite isochron (Smoliar *et al.*, 1996). The IIIA isochron is the horizontal line at $\Delta_{\text{Os}} = 0$. Analytical uncertainties are either shown or are smaller than the symbols.

Table 4: Os isotopic compositions of Johnson Matthey Os Standard, and two Allende CAIs. All Os isotopic data were normalized to ^{189}Os and corrected for fractionation using $^{192}\text{Os}/^{189}\text{Os}=2.527411$. Analytical uncertainties of individual runs are 2σ , and external precision for average is 2σ . The 2σ uncertainties are for the last few digits of the reported values.

Standards	$^{186}\text{Os}/^{189}\text{Os}$	2σ	$^{187}\text{Os}/^{189}\text{Os}$	2σ	$^{188}\text{Os}/^{189}\text{Os}$	2σ	$^{190}\text{Os}/^{189}\text{Os}$	2σ
Os std 1 (70ng)	0.0982661	94	0.0932963	92	0.8199060	293	1.6263832	343
Os std 2 (70ng)	0.0982672	120	0.0932952	118	0.8199087	366	1.6263790	410
Os std 3 (70ng)	0.0982621	126	0.0932937	119	0.8199061	348	1.6263693	416
Average	0.0982651	544	0.0932951	274	0.8199069	38	1.6263772	87

CAIs	$^{188}\text{Os}/^{189}\text{Os}$	2σ	$\varepsilon^{188}\text{Os}$	2σ	$^{190}\text{Os}/^{189}\text{Os}$	2σ	$\varepsilon^{190}\text{Os}$	2σ
3529-35	0.8199151	341	0.100	79	1.6263701	398	-0.043	92
19B65	0.8199059	503	-0.013	117	1.6263859	555	0.054	129

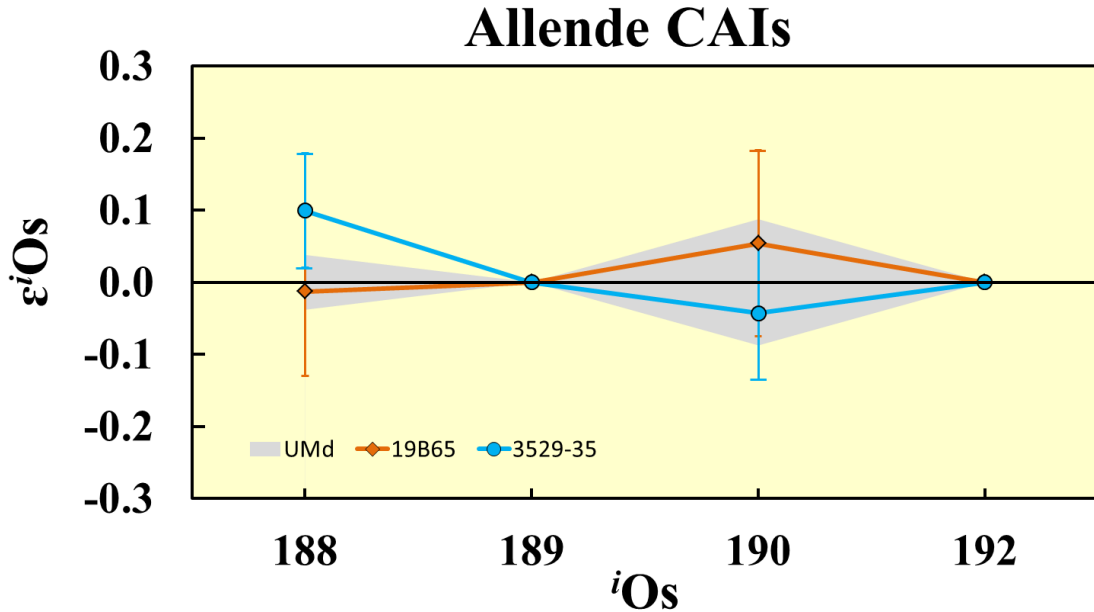


Figure 28: Os isotopic composition of Allende CAIs. $\varepsilon^i\text{Os}$ represents deviations from a terrestrial standard. The external reproducibility of the standard is represented by the grey field.

Chapter 5: Discussion

5.1 Rare Earth Elements

5.1.1 Condensation of REE in CAIs

Five of the six REE patterns of second suite CAIs have REE patterns that are essentially unfractionated relative to bulk chondrites (Figures 17a, 17b, and 17d). These unfractionated patterns indicate that the REE, except for the most volatile, Eu and Yb, were completely condensed in these CAIs in one condensation event. This interpretation is consistent with conclusions made by previous studies (e.g., Grossman, *et al.* 1977; Grossman, 1980). In contrast, the REE pattern of 18B61 is highly fractionated (Figure 17c), consistent with REE patterns of other group II CAIs (e.g., Mason & Taylor, 1982). Davis & Grossman (1979) used thermodynamic calculations to show that group II REE patterns are the result of fractional condensation, during which a component with the most refractory REE condensed and was removed, and then the remaining REE, except for the most volatile, within the gas residue condensed. The REE pattern of 18B61 is consistent with this fractional condensation model for group II CAIs.

5.1.2 Minor Differences of REE Patterns in Second Suite CAIs Compared to Previous Studies

There are some differences in the REE patterns of CAIs measured in this study from CAIs for which data have been previously reported (e.g., from Mason & Taylor, 1982). The REE pattern of 7B75 has a well resolved positive Eu anomaly, which defines it as a group I CAI, but its absolute abundances of REE are much lower than the other type I CAIs in the data set (Figure 17b). This may be a result of dominantly sampling a

REE-poor phase, such as spinel, which would have a dilutional effect. However, this dilutional effect would only reduce the absolute abundances of the REE, and would not affect the relative abundances of the REE. Thus, despite the absolute abundances being lower, the relative abundances of the REE must still reflect those of the bulk CAI.

The only group II CAI identified here, 18B61, has lower absolute abundances of REE than most previously reported group II CAIs. Typically, abundances of the LREE in group II CAIs are about 30x to 60x chondritic abundances, whereas 18B61 has abundances of LREE of about 8x chondritic. This CAI has a positive Eu anomaly, whereas most group II CAIs have negative Eu anomalies (Mason & Taylor, 1982). The data for this CAI are not unique, however. Mason & Taylor (1982) reported data for one Allende CAI, 5242, characterized by similarly low absolute abundances of the LREE and a positive Eu anomaly. There are other instances of group II CAIs having positive Eu anomalies (Conard, 1976; Grossman & Ganapathy, 1976) Positive Eu anomalies of some group II CAIs is most likely a result of preferential sampling of a Eu-rich phase, (e.g., melilite).

5.2 Highly Siderophile Elements in Chondritic Components

5.2.1 Highly Siderophile Elements in CAIs

The non-group II CAIs analyzed by this study have enriched but flat chondrite-normalized abundance patterns for the most refractory HSE (Re, Os, Ir, Ru, and Pt). This is consistent with high temperature condensation of these elements. However, all non-group II CAIs have major depletions in the most volatile HSE, Pd. This indicates that this fractionation is most likely due to the volatility of Pd. Mason & Taylor (1982)

reported a data set in which both Pd and Rh (Rh is an HSE with a similar 50% condensation temperature to that of Pd) had major depletions in non-group II CAIs. They interpreted these depletions as being directly related to the volatilities of these elements. Previous studies have demonstrated that depletions of moderately volatile elements are correlated with their condensation temperatures (e.g., Cassen, 1996).

At some point in their formation histories, CAIs (or their precursors) were isolated from the gas from which they were condensing (Davis & Richter, 2003). Any elements that had not already condensed by that point would be depleted in CAIs. Thus, the Pd depletions found in CAIs could be the result of separating CAIs or their precursors from solar nebular gas above the 50% condensation temperature of Pd (1324 K at 10^{-4} bar).

Another possible explanation for Pd depletions is evaporative loss of Pd during a heating event. Some CAIs show evidence of heating and evaporative loss of Si and Mg, as well as evaporative loss of light Si and Mg isotopes (Clayton *et al.*, 1988; Grossman *et al.*, 2000). Palladium, Si, and Mg have similar 50% condensation temperatures between 1360-1290 K (Lodders, 2003). Therefore, the heating event that caused Mg and Si to evaporate would have likely also caused Pd to evaporate and become depleted in CAIs.

5.2.2 Refractory HSE-rich Precursor

Chondrules show a wide variation in HSE abundances relative to bulk chondrites (Figure 20). For example, three of the Allende chondrules measured by this study are enriched in Re, Os, Ir, Ru, and Pt relative to bulk Allende, whereas three are depleted in those same elements, as well as Pd. Four out of the six chondrules also show relative Pd

depletions. One of the precursor components of chondrules in CV chondrites is a refractory high-temperature condensate (Grossman & Wasson, 1982; Grossman & Wasson, 1985). This component is essentially composed of fragments of CAIs, and would, therefore, be enriched in Re, Os, Ir, Ru and Pt, relative to bulk Allende. It is likely that some chondrules were formed with different proportions of this precursor material (e.g., Misawa & Nakamura, 1996). Thus, chondrules may have either refractory HSE enriched, or depleted abundances, relative to bulk Allende, based on the fraction of high-temperature condensate precursor material that was included in the aggregates that melted and formed the chondrules. Given that CAIs are characterized by Pd depletions relative to bulk Allende, this conclusion is also consistent with the negative Pd depletions observed in most of the chondrules analyzed by this study.

5.2.3 Two HSE-bearing Components

Another possible explanation for the variable HSE abundances in chondrules stems from the incorporation of two different HSE carrier phases. Horan *et al.* (2009) described two different carrier phases for HSE in chondrules from ordinary chondrites. One component was magnetic and characterized by unfractionated HSE, relative to the bulk meteorite. The other component was non-magnetic and characterized by fractionated (depleted in Re and Pd) HSE, relative to the bulk meteorite. They presented an argument that Pd depletions present in the nonmagnetic fraction could be the result of solid metal-liquid metal fractionation of HSE during metal melting in the presence of high S, as Pd is incompatible in high S systems (Chabot & Jones, 2003). For this model, the nonmagnetic fraction essentially contains a residue of metal melts, and this melting is

associated with chondrule formation. The bulk chondrule data reported here are consistent with a mixture of the two components as evidenced by variable Pd depletions. If the mixture of these two materials is responsible for the HSE abundance patterns seen in chondrules, the high variation in absolute abundances of HSE could be the result of different proportions of the two HSE carriers within each chondrule.

One issue in appealing to the two HSE-bearing components found by Horan *et al.* (2009) in ordinary chondrites is the assumption that the HSE characteristics of Allende, an oxidized CV, can be directly compared to the HSE characteristics of ordinary chondrites. Caveats of this assumption include the following: (1) the existence, or at least former existence, of the magnetic, metallic, HSE-rich component in Allende chondrules, and (2) the high-S required to fractionate Pd via solid metal-liquid metal interaction during the production of an HSE-poor component in Allende chondrules during chondrule formation.

Concerning the first stipulation, Allende chondrules are characterized by very little metal. However, bulk Allende has around 1% magnetite (Hyman & Rowe, 1983), and most of the magnetite in Allende is contained within chondrules. This magnetite probably formed during oxidation of metal in the parent body (i.e., asteroidal rather than nebular alteration) (Krot *et al.*, 1995). Thus, although the metal in these chondrules was converted to magnetite after chondrule and parent body formation, the HSE budget from the inherited metal would already have been imparted to the chondrule. Concerning the second requirement, previous studies have shown that sulfur abundances (about 2%) of Allende are similar to those of ordinary chondrites (Dreibus *et al.*, 1995). Therefore, there is no reason to assume, based on lack of S, that the solid metal-liquid metal

interaction that may have caused Pd depletions in the nonmagnetic component in ordinary chondrite chondrules could not have also caused Pd depletions in a nonmagnetic component of Allende chondrules.

The most compelling piece of evidence that indicates Allende chondrules can be compared to ordinary chondrite chondrules, in terms of two HSE-bearing components, is the similarity in HSE abundance patterns for Allende chondrules and those of ordinary chondrite Chainpur (Figure 22). If the processes that established the HSE patterns for ordinary chondrite chondrules and Allende chondrules were not similar, it is probable that the patterns would not show such striking similarities.

5.2.4 Highly Siderophile Elements in Matrix

The abundance patterns of matrix materials are generally similar to those of bulk Allende. However, the Allende matrix is characterized by higher Pd abundances than bulk Allende. Palladium abundances of matrix vary by a factor of ~1.6 among different analyzed matrix fractions. Two of the four patterns do not show Pd depletions relative to bulk Allende. Unlike chondrules, the lack of Pd depletions in the abundances of HSE in these matrix data are not consistent with a mixture containing a fractionated (Pd-depleted) HSE component, and are instead consistent with matrix HSE patterns being dominated by only a single, unfractionated HSE component.

In terms of HSE mass balance within Allende, the relative Pd enrichment in matrix may account for most of the bulk abundance of Pd in Allende (CAIs and chondrules show relative Pd depletions relative to bulk Allende). If the abundances of bulk Allende are modeled using the mean Pd abundances of three components, CAIs,

chondrules, and matrix, as well as the proportions of these components in Allende, a value of 485 ppb is calculated. This value only represents about 70% of the total abundance of Pd in Allende. However, this calculation is complicated by the high degree of variability in Pd abundances within individual components. For example, chondrules vary by a factor of ~116 in Pd abundances. Therefore, if the calculated mean value of Pd for either CAIs, chondrules, or matrix has been driven down by more low-Pd abundance component fractions than is representative of bulk Allende, then this could account for the low calculated model abundance of Pd in bulk Allende. Also, the Pd abundances of amoeboid olivine aggregates (AOA) are currently unknown, and this component makes up 3.2% of Allende. If AOAs have suprachondritic Pd abundances, their inclusion in mass balance calculations of bulk Allende would drive the calculated Pd abundance from individual components closer to the bulk Allende Pd abundances provided by previous studies (e.g., Horan *et al.*, 2003).

5.3 Rhenium-Osmium Isotope Systematics in Chondritic Components

Most of the fractions of CAIs, chondrules, and matrix analyzed by this study do not plot on a primordial isochron. Becker *et al.* (2001) reported Re-Os isotope systematics of Allende CAIs in which 8 out of 24 bulk CAIs and fractions of CAIs plotted off of a primordial isochron within uncertainty. There are several possible explanations for this apparent non-isochronous behavior. These include analytical issues, early solar system processes, and late-stage open system behavior. Each of these possibilities is discussed as follows.

5.3.1 Analytical Issues

For the chondritic components analyzed in this study, it is not likely that analytical issues or contamination from other materials had any influence on the deviations of these components from the primordial isochron. The main analytical issues that could cause apparent non-isochronous behavior in CAIs are random blank problems (overestimation or underestimation of Re or Os blanks) and incomplete digestion of HSE carrier phases (preferential leaching of either Re or Os).

All measured Os blanks were generally low, with blank corrections typically less than 0.1%, which is not sufficiently high enough to account for the non-isochronous behavior of the chondritic materials measured by this study. For non-group II CAIs, all observed Re blank contributions were less than 1% and typically less than 0.5%. Also, most of the non-group II CAIs that do not plot on a primordial isochron plot to the left of the primordial isochron. If the Re blank was underestimated for any of these samples, it would drive the apparent $^{187}\text{Re}/^{188}\text{Os}$ to the right of the primordial isochron. Therefore, underestimation of Re blanks is not likely the cause for non-isochronous behavior in these CAIs.

Conversely, overestimation of Re blanks would cause calculated $^{187}\text{Re}/^{188}\text{Os}$ to be lower than the real value and data points would plot to the left of the primordial isochron. However, even if it is assumed there was no input of Re from the blank these samples would still plot to the left of the primordial isochron. Therefore, underestimation of blanks is also not a likely cause for non-isochronous behavior of these CAIs.

For the group II CAI 3529-40, the measured Re blank was about 7% of the Re measured in the CAI due to the lower abundance of Re in this CAI compared to non-

group II CAIs. Also, this CAI plots to the right of a primordial isochron. Therefore, underestimation of the Re blank for this sample cannot be excluded as the cause for the non-isochronous behavior of this CAI.

For chondrules, Re blank corrections were typically less than 1% of total Re measured, although one chondrule, Al A, had a large, 7% correction. However, Al A plots to the left of the primordial isochron, and underestimation of the Re blank would cause it to plot to the right of the primordial isochron. Therefore, underestimation of the Re blank cannot be the cause of non-isochronous behavior for Al A. If, however, the Re blank is assumed to be negligible for Al A, then the data for this chondrule plots close to a primordial isochron, and overestimation of the Re blank cannot be excluded as the reason for the apparent non-isochronous behavior of Al A. For all other chondrules, overestimation or underestimation of the Re blank cannot account for their non-isochronous behavior.

Rhenium blank corrections for matrix were all less than 4%, and 2 out of four were less than 1%. Most matrix analyses plot to the left of the primordial isochron, therefore, underestimation of the blank cannot account for the non-isochronous behavior of matrix. If a negligible blank is assumed for all matrix components, they still do not plot on a primordial isochron, therefore, overestimation of the blank cannot be the cause of the non-isochronous behavior of these matrix analyses.

It is possible that incomplete dissolution of Re- or Os-bearing phases could cause deviations about the isochron. However, the Carius tube digestion method discussed in this paper is a highly efficient way of accessing Re- and Os- bearing phases with low blank contributions (Shirey and Walker, 1995; Walker *et al.*, 2002). Also, preferential

leaching of Re- or Os-bearing phases would cause correlated shifts of $^{187}\text{Re}/^{188}\text{Os}$ and $^{187}\text{Os}/^{188}\text{Os}$ data along the primordial isochron, and would not cause apparent non-isochronous behavior (Becker *et al.*, 2001). This is due to the Re decay product, ^{187}Os , being contained in Re-rich phases. Therefore, if Re was not sufficiently accessed, then the calculated $^{187}\text{Re}/^{188}\text{Os}$ would be lower; however, the ^{187}Os associated with the Re would also not be accessed, which would cause a correspondingly lower $^{187}\text{Os}/^{188}\text{Os}$.

5.3.2 Early Solar System Processes

Early solar system isotopic heterogeneities are an unlikely cause of the non-isochronous behavior seen here. If the initial $^{187}\text{Os}/^{188}\text{Os}$ of the Allende materials was somehow significantly affected by nucleosynthetic affects or incomplete mixing of the early solar system, then other isotopes of Os would be affected similarly. However, based on unspiked Allende CAIs that were analyzed by this study, there is no evidence that nucleosynthetic processes changed the initial $^{187}\text{Os}/^{188}\text{Os}$ of CAIs, especially to the degree necessary to cause the apparent non-isochronous behavior seen in Allende CAIs (Figure 28). Also, the Re isotopic compositions of unspiked Allende CAI analyses do not show large deviations from terrestrial standard Re isotopic compositions, therefore early solar system isotopic heterogeneities of Re are also not likely the cause of the observed non-isochronous behavior of Allende components.

Fractionation of Re and Os in the early solar system is also not likely the cause of the non-isochronous behavior of the chondritic components analyzed by this study (Becker *et al.*, 2001). In order for this to be the case, Re and Os would have to have first been fractionated, resulting in a suprachondritic $^{187}\text{Re}/^{188}\text{Os}$. Then, the Re-Os system

would have to have been closed for hundreds of thousands or millions of years, followed by another fractionation event that would have to have reversed the Re-Os isotope system back to the near chondritic values measured by this study. This complex sequence of events is unlikely to be the cause of the apparent non-isochronous behavior seen in chondritic components.

5.3.3 Late stage Open-System Behavior

The most likely reason these chondritic components plot off of a primordial isochron is terrestrial or parent-body late stage open-system behavior, with Re and/or Os being mobilized. Becker *et al.* (2001) reported that data for a single CAI 3529-41 defined an internal errorchron age of 1614 ± 39 Ma. They interpreted this errorchron as dating an event in which the Re-Os system was disturbed. The data presented here support this interpretation, as multiple CAIs, chondrules, and matrix fractions plot along this 1614 ± 39 Ma errorchron. This is the first study that has found a correlation between the non-isochronous Re-Os behavior of CAIs and other Allende components.

There is evidence for late stage open-system behavior in other radiogenic isotope systems. For example, Grey *et al.* (1973), Tatsumoto *et al.* (1976), and Podosek *et al.* (1991) found evidence for open-system behavior in Rb-Sr systematics for Allende chondritic components that occurred earlier than 3.6 Ga. There is evidence for late stage (<300 Ma) open-system behavior of U-Pb systematics in Allende components (Chen & Tilton, 1976; Tatsumoto *et al.*, 1976; Chen & Wasserburg, 1981). There is also evidence for open-system behavior of the Sm-Nd system; however, previous studies have not provided time constraints for this behavior (Papanastassiou *et al.*, 1987; Bogdanovski &

Jagoutz, 1999). There is currently no correlation between the time constraints of open-system behavior of the Re-Os isotope system and other isotope systems that show apparent open-system behavior. One possibility is that these systems have different vulnerabilities to open-system behavior, and some alteration events have only caused open-system behavior in some systems. Thus, one event may have caused Allende components to plot on a 1614 ± 39 Ma Re-Os isochron, and this event has been overprinted in, for example, U-Pb systematics by a more recent event so that some Allende components intercept a U-Pb concordia diagram at a younger age, rather than the age determined by Re-Os. If this is the case, Re-Os isotope systematics would have to be more resistant to open-system behavior than U-Pb isotope systematics.

Xiong and Wood (1999) demonstrated that in experimental hydrothermal fluids, Re and Os have different mobilities. Thus, it is possible that a late-stage event, possibly the collision of the Allende parent body with another asteroid, caused the fluid mobilization and the preferential transport of Re over Os. Based on the correlated deviations found in chondritic components analyzed by this study, this explanation seems to be the most likely.

If late-stage open system behavior caused Re to be preferentially transported over Os, there should be some fractions of Allende components with enriched $^{187}\text{Re}/^{188}\text{Os}$ without a correspondingly high $^{187}\text{Os}/^{188}\text{Os}$. One of the matrix analyses provided by this study shows a highly elevated $^{187}\text{Re}/^{188}\text{Os}$ of 0.7213 ± 0.0035 , however the $^{187}\text{Os}/^{188}\text{Os}$ of 0.12679 is similar to the $^{187}\text{Os}/^{188}\text{Os}$ of bulk Allende. The elevated $^{187}\text{Re}/^{188}\text{Os}$ of this sample without a correspondingly high $^{187}\text{Os}/^{188}\text{Os}$ indicates that the $^{187}\text{Re}/^{188}\text{Os}$ was enriched recently, without enough time to significantly enrich the $^{187}\text{Os}/^{188}\text{Os}$. This lends

further support to the conclusion that Allende underwent late-stage open system behavior with Re movement.

5.3.4 Higher Degree of Variation in Smaller Samples

This study provides a data set in which the majority of CAI fractions (13 out of 14) plot off of a primordial isochron within uncertainty, whereas a lower proportion (8 out of 24) of CAI fractions from Becker *et al.*, (2001) did not plot on a primordial isochron. One major difference between the samples analyzed by this study and those of Becker *et al.* (2001) is sample size. The bulk CAIs and CAI fractions analyzed by Becker *et al.* (2001) were, on average, 40 mg, whereas the CAI fractions here were, on average, 3 mg. Therefore, it seems that that non-isochronous behavior may be more easily resolved in smaller scale fractions of CAIs. This is consistent with local transport of Re because of late-stage open system behavior.

5.3.5 Modeling Re-Os Systematics of Bulk Allende Using Components

Using the Re-Os Allende component data compiled in this study in conjunction with those data presented in Becker *et al.* (2001), model bulk $^{187}\text{Re}/^{188}\text{Os}$ and $^{187}\text{Os}/^{188}\text{Os}$ were calculated for Allende. Due to unknown parameters (i.e., proportion of non-group II CAIs vs. group-II CAIs), the means were not corrected for the proportions of each component in Allende. Rather, each analysis was weighted equally, irrespective of the type of component. Therefore, it must be noted that the model is heavily skewed towards CAI Re-Os isotope systematics; however, non-group II CAIs are the dominant carrier of Re and Os and generally have at least an order of magnitude greater abundances of Re

and Os than chondrules and matrix. These calculated values for bulk Allende are 0.12635 and 0.3883, for $^{187}\text{Re}/^{188}\text{Os}$ and $^{187}\text{Os}/^{188}\text{Os}$, respectively. A comparison of this model value with previously reported values for bulk Allende (Walker *et al.*, 2002) indicates that, although small-scale components show non-isochronous behavior, when combined together, the components plot very close to a primordial isochron (Figure 29).

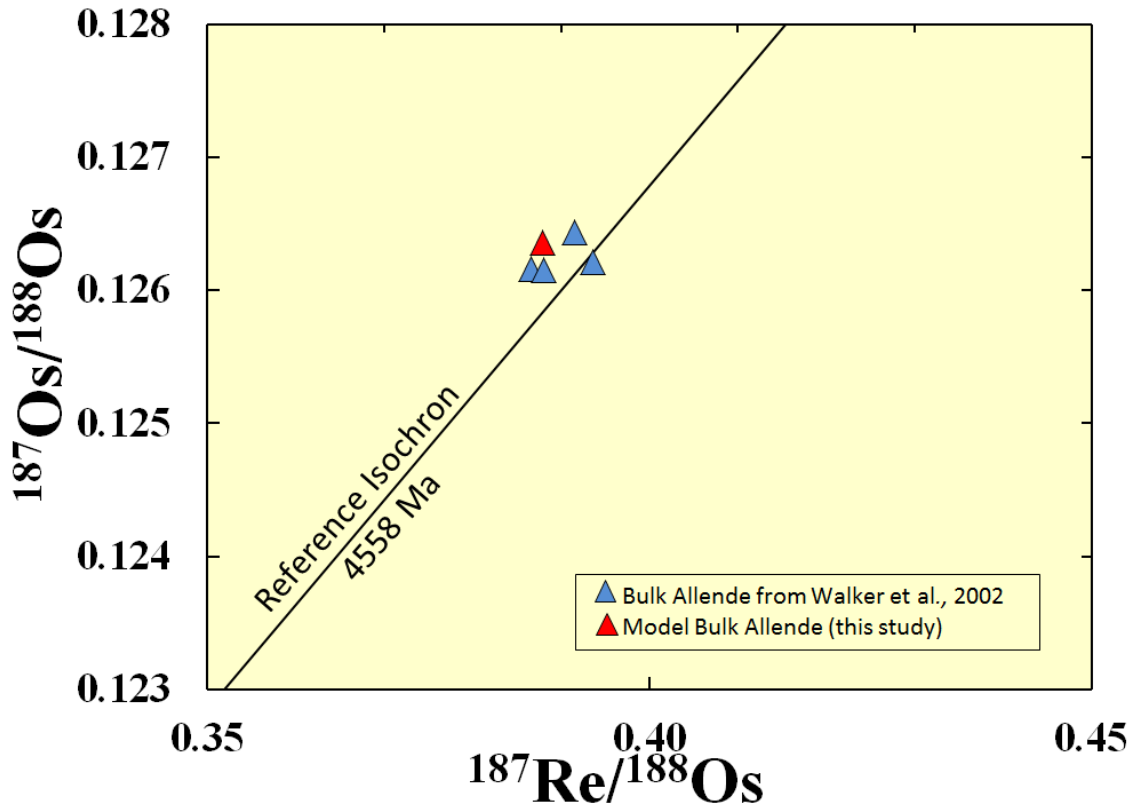


Figure 29: Re-Os systematics of bulk Allende. Model bulk Allende calculated from all components of this data set combined with data from Becker *et al.* (2001). Data for bulk Allende taken from Walker *et al.* (2002) in which whole-rock analyses of Allende

Chapter 6: Synthesis

The examination of REE abundances, HSE abundances, Re-Os systematics, Re isotopic compositions, and Os isotopic compositions of chondritic components allowed several interesting conclusions to be drawn about the early solar system, chondrite component formation, post-formation processes that affected Allende and possibly other chondrites, and the isotopic compositions of Re and Os in the early solar system.

This study was designed to accomplish the following: (1) classify several recently separated Allende CAIs using REE abundances, (2) determine the HSE abundances of chondritic components (CAIs, chondrules and matrix), (3) further assess open-system behavior of multiple chondritic components in the Allende parent body using the Re-Os isotope system, (4) determine whether or not the Re isotopic compositions of Allende CAIs were altered by cosmic ray interactions, and (5) investigate possible Os nucleosynthetic anomalies in CAIs.

Based on REE abundance patterns, several recently separated Allende CAIs are classified into groups by this study. Three of the CAIs have group I patterns. One CAI has a highly fractionated group II pattern. Two CAIs have group III patterns. The group II patterns are consistent with fractional condensation, whereas the non-group II patterns are consistent with a single condensation event in which all of the most refractory HSE condensed (Grossman *et al.*, 1977; Davis & Grossman, 1979; Grossman, 1980). The REE patterns of two of the CAIs have minor differences with previously reported REE abundance patterns, which can be attributed to preferentially sampling specific phases within the CAIs.

Previous studies have concluded that HSE abundances in CAIs are related to the different volatilities of individual HSE (Mason & Taylor, 1982). The non-group II CAIs measured by this study are characterized by flat, but enriched chondrite-normalized abundance patterns for the most refractory HSE (Re, Os, Ir, Ru, and Pt), and large depletions in the most volatile HSE, Pd. The Pd depletions of non-group II CAIs indicate that either (1) CAIs were separated from the gas from which they were condensing at a temperature above the 50% condensation temperature of Pd, or (2) CAIs experienced a heating and evaporation event that removed Pd. Also, Pd concentrations determined by this study are consistently lower than previously reported values (Mason & Taylor, 1982). Even data from individual non-group II CAIs that were analyzed both by this study and by previous studies have discrepancies. Therefore, the differences are most likely the result of analytical issues.

Chondrules have highly variable absolute HSE abundances; however, their chondrite-normalized HSE patterns are generally flat (except for Pd), and are either slightly enriched or depleted in the more refractory HSE relative to bulk chondrites. Like CAIs, chondrules also have Pd depletions. These Pd depletions may be the result of either (1) incorporation of a CAI-like precursor, or (2) incorporation of two different HSE bearing components, a fractionated-HSE, nonmagnetic component and an unfractionated-HSE, magnetic component. The components mentioned in (2) have been found in chondrules from ordinary chondrites analyzed by a previous study (Horan *et al.*, 2009).

Matrix fractions do not show Pd depletions, which indicates that the HSE in matrix are dominated by a single, unfractionated-HSE component. In terms of mass balance, it is possible that matrix material contains the majority of the budget of Pd found

in bulk Allende. However, modeling calculations done by this study can only account for 70% of the Pd found in bulk Allende. It is possible that a component, perhaps amoeboid olivine aggregates, for which there is currently no HSE data, has a large fraction of the Pd that is contained in bulk Allende.

Most of the CAIs, chondrules, and matrix fractions analyzed by this study do not plot on a primordial isochron. Analytical issues, early solar system fractionation of Re & Os, and early solar system isotopic heterogeneities of Re or Os are unlikely the cause. The most likely reason for the apparent non-isochronous behavior is late stage open-system behavior, during which the Re-Os isotope system was disturbed. Several CAIs, chondrules, and matrix fractions define a linear array that corresponds to an age of 1614 Myr. Therefore, it is possible that the Re-Os isotope systematics of these chondritic components provide an age constraint for some event that caused open-system behavior.

A bulk Allende Re-Os model calculated by combining the Re-Os systematics of the individual components indicates that, although individual components show non-isochronous behavior, when combined together, the bulk Allende model plots close to a primordial isochron. Also, a comparison between larger CAI samples (on average, 40 mg) measured by Becker *et al.*, (2001), and smaller CAI samples (on average, 3 mg) measured by this study indicates that a greater fraction of small CAI samples show non-isochronous behavior compared to larger CAI samples. These two observations indicate that the mobility of Re or Os during open-system behavior happened on a small, likely mm, scale.

The stable isotopic compositions of Re and Os in CAIs indicate that there are small differences between the Re isotopic composition of CAIs and a terrestrial standard.

However, it is unclear what the source of these differences is. The differences in Re isotopic composition between CAIs and a terrestrial standard are not large enough to account for the non-isochronous behavior of these CAIs. The Os isotopic composition of CAIs is indistinguishable, within uncertainty, of a terrestrial standard, which indicates that CAIs do not contain Os nucleosynthetic anomalies.

References

- Alexander C. M. O'D., Boss A. P., and Carlson R. W. (2001) The early evolution of the inner solar system: a meteoritic perspective. *Science* **293**, 64–68.
- Allen J.M., Grossman, L., Lee T., Wasserburg G.J. (1980) Mineralogy and petrology of HAL, an isotopically unusual Allende inclusion. *Geochim. Cosmochim. Acta* **44**, 685-699.
- Amelin Y., Krot A. N., Hutcheon I.D., and Ulyanov A. A. (2002) Lead isotopic ages of chondrules and calcium-aluminum-rich inclusions. *Science* **297**, 1678-1683.
- Arlandini, C., Kappeler, F., Wisshak, K., Gallino, R., Lugardo, M., Busso, M., Straniero, O. (1999) Neutron capture in low-mass asymptotic giant branch stars: cross sections and abundance signatures. *Astrophys. J.* **525**, 886–900.
- Becker H., Walker R.J., and Morgan J.W. (1999) Re-Os isotopic systematics of matrix, chondrules, metal and more CAIs from the Allende meteorite. *Lunar Planet Sci. Conf.* **XXIX**, 1086.
- Becker H., Morgan J. W., Walker R. J., MacPherson G. L. and Grossman J. N. (2001) Rhenium–osmium systematics of calcium–aluminum-rich inclusions in carbonaceous chondrites. *Geochim. Cosmochim. Acta* **65**, 3379–3390.

Birck, J.L., Barman, M.R., Capmas, F. (1997) Re–Os isotopic measurements at the femtomole level in natural samples. *Geostand. Newslet.* **21**, 19–27.

Bogdanovski O. and Jagoutz E. (1999) Samarium-neodymium isotopic systematics of CAIs from Efremovka and Allende meteorites. *Lunar Planet. Sci. Conf.* **XXX**, 1891.

Bouvier A., and Wadhwa M. (2010) The age of the Solar System redefined by the oldest Pb-Pb age of a meteorite inclusion. *Nature Geoscience* **3**, 637-641.

Boynton W. V. (1975) Fractionation in the solar nebula: condensation of yttrium and the rare earth elements. *Geochim. Cosmochim. Acta* **39**, 569–584.

Brearley A. J. and Jones R. H. (1998) Chondritic meteorites. In Planetary Materials (J. J. Papike ed.). *Rev. Mineral.* **36**, 3-01–3-398.

Brennecka, G.A., Borg, L.E., Wadhwa, M. (2011) Barium, neodymium, and samarium isotope compositions of Allende CAIs. *Lunar Planet. Sci. XXXII*, 1302.

Burkhardt, C. *et al.* (2011) The Molybdenum Isotopic Composition of meteoritic metals: evidence for planetary scale isotope heterogeneity of the solar nebula. *Lunar Planet. Sci. XXXI*, 2131.

Caillet C.A. (1994) A new type of Al-rich inclusion in Axtell CV3 chondrite. *Meteoritics* **29**, 453-454.

Cassen P. (1996) Models for the fractionation of moderately volatile elements in the solar nebula. *Meteorit. Planet. Sci.* **31**, 793–806.

Chabot N. L. and Jones J. H. (2003) The parameterization of solid metal–liquid metal partitioning of siderophile elements. *Meteoritics Planet. Sci.* **37**, 1425–1436.

Chen J. H. and Tilton G. R. (1976) Isotopic lead investigations on the Allende carbonaceous chondrite. *Geochim. Cosmochim. Acta* **40**, 635–643.

Chen J. H. and Wasserburg G. J. (1981) The isotopic composition of uranium and lead in Allende inclusions and meteoritic phosphates. *Earth Planet. Sci. Lett.* **52**, 1–15.

Chen, J.H., Papanastassiou, D.A., Wasserburg, G.J. (2010) Ruthenium endemic isotope effects in chondrites and differentiated meteorites. *Geochim. Cosmochim. Acta* **74**, 3851-3862.

Clark R.S., Jarosewich E., Mason B., Nelen J., Gómez. M, and Hyde J.R. (1970) The Allende Mexico meteorite shower. *Smithsonian Contrib. Earth Sci.* **5**, 1-53

Clayton R. N., Onuma N., and Mayeda T. K. (1976) A classification of meteorites based on oxygen isotopes. *Earth and Planetary Science Letters* **30**, 10-18.

Clayton R. N., Hinton R. W., and Davis A. M. (1988) Isotopic variations in the rock-forming elements in meteorites. *Phil. Trans. Roy. Soc. London A* **325**, 483–501.

Cohen A. S. and Waters F. G. (1996) Separation of osmium from geological materials by solvent extraction for analysis by thermal ionisation mass spectrometry. *Anal. Chim. Acta* **332**, 269–275

Conard, R. (1976) A study of the chemical composition of Ca-Al-rich inclusions from the Allende meteorite. M.S. thesis. Oregon State Univ., Corvallis.

Connolly Jr. H. C., Huss G. R., and Wasserburg G. J. (2001) On the formation of Fe-Ni metal in Renazzo-like carbonaceous chondrites. *Geochim. Cosmochim. Acta* **65**, 4567-4588.

Connelly, J., Amelin, Y., Krot, A. N. & Bizzarro, M. (2008) Chronology of the Solar System's oldest solids. *Astrophys. J. Lett.* **675**, L121-L124.

Davis A. M. and Grossman L. (1979) Condensation and fractionation of rare earths in the solar nebula. *Geochim. Cosmochim. Acta* **43**, 1611–1632.

Davis A. M., Tanaka T., Grossman L., Lee T., and Wasserburg G. J. (1982) Chemical composition of HAL, an isotopically unusual Allende inclusion. *Geochim. Cosmochim. Acta* **46**, 1627–1651.

Davis A. M. and Richter F. M. (2003) *in Meteorites, Planets, and Comets, Vol. 1, Treatise on Geochemistry* (HD Holland, KK Turekian eds) (Oxford: Elsevier-Pergamon), 201-246.

Desch S. J. and Cuzzi J. N. (2000) The generation of lightning in the solar nebula. *Icarus*, **143**, 87–105.

Desch S. J. and Connolly H. C. Jr. (2002) A model of the thermal processing of particles in solar nebula shocks: Application to the cooling rates of chondrules. *Meteoritics & Planet. Sci.*, **37**, 183–207.

Desch S. J., Ciesla F. J., Hood L. L. and Nakamoto T. (2005) Heating of chondritic materials in solar nebula shocks. *In Chondrites and the Protoplanetary Disk*, vol. 341 (A. N. Krot, E. R. D. Scott and B. Reipurth eds). ASP Conference Series, pp. 849–873.

Dreibus G., Palme H., Spettel B., Zipfel J., and Wanke H. (1995) Sulfur and selenium in chondritic meteorites *Meteoritics* **30**, 439-445.

Ebel D. S. and Grossman L. (2000) Condensation in dust-enriched systems. *Geochim. Cosmochim. Acta* **64**, 339–366.

Fischer-Gödde M., Becker, H., and Wombacher F. (2010) Rhodium, gold and other highly siderophile element abundances in chondritic meteorites *Geochim. Cosmochim. Acta* **74**, 356-379.

Gooding J. L. and Keil K. (1980) Relative abundances of chondrule primary textural types in ordinary chondrites and their bearing on conditions of chondrule formation. *Meteoritics* **16**, 17-43.

Gounelle M., Shu F. H., Shang H., Glassgold A. E., Rehm E. K., and Lee T. (2001) Extinct radioactivities and protosolar cosmic rays: self-shielding and light elements *Astrophys. J.* **548**, 1051

Gray C. M., Papanastassiou D. A., and Wasserburg G. J. (1973) The identification of early condensates from the solar nebula. *Icarus* **20**, 213–239.

Grossman L. (1972) Condensation in the primitive solar nebula. *Geochem. Cosmochim. Acta* **36**, 597-619.

Grossman L., Clark Jr. S. P. (1973) High-temperature condensates in chondrites and the environment in which they formed. *Geochim. Cosmochim. Acta* **37**, 635-649.

Grossman L. (1975) Petrography and mineral chemistry of Ca-rich inclusions in the Allende meteorite. *Geochim. Cosmochim. Acta* **39**, 433-453.

Grossman L. and Ganapathy R. (1976) Trace elements in the Allende meteorite -I. Coarse-grained, Ca-rich inclusions. *Geochim. Cosmochim. Acta* **40**: 331-344.

Grossman L., Ganapathy R., and Davis A. M. (1977) Trace elements in the Allende meteorite-III. Coarse-grained inclusions revisited *Geochim. Cosmochim. Acta* **41**: 1647-1664.

Grossman L. (1980) Refractory Inclusions in the Allende Meteorite. *Annual Review of Earth and Planetary Science* **8**, 559-608.

Grossman J.N. and Wasson J.T. (1982) Evidence for primitive nebular components in chondrules from the Chainpur chondrite. *Geochim. Cosmochim. Acta* **46**, 1081-1099.

Grossman J. N. and Wasson J. T. (1985) The origin and history of the metal and sulfide components of chondrules. *Geochim. Cosmochim. Acta* **49**, 925-939.

Grossman J.N., Rubin A.E., Nagahara H., King E.A. (1988) Properties of chondrules. In Meteorites and the Early Solar System (JF Kerridge, MS Matthews eds) University of Arizona Press, 619-659

Grossman L., Ebel D. S., Simon S. B., Davis A. M., Richter F. M., and Parsad N. M. (2000) Major element chemical and isotopic compositions of refractory inclusions in C3 chondrites: the separate roles of condensation and evaporation. *Geochim. Cosmochim. Acta* **64**, 2879–2894.

Horan M. F., Walker R. J., Morgan J. W., Grossman J. N. and Rubin A. (2003) Highly siderophile elements in chondrites. *Chem. Geol.* **196**, 5–20.

Horan M. F., Alexander C.M.O'D., and Walker R. J. (2009) Highly siderophile element evidence for early solar system processes in components from ordinary chondrites. *Geochim. Cosmochim. Acta* **73**, 6984-6997.

Humayan M., Connolly Jr. H. C., Rubin A. E., Wasson J. T. (2010) Elemental distribution of metal from the CR chondrites Acfer 059 and PCA 91082. *Lunar Planet. Sci. XXXI*, 1840.

Hyman M. and Rowe M. W. (1983) The origin of magnetite in carbonaceous chondrites (abstract), *Lunar Planet. Sci.* **14**, 341-342.

Ireland T. R., Fahey A. J., and Zinner E. K. (1988) Trace element abundances in hibonites from the Murchison carbonaceous chondrite: constraints on high-temperature processes in the solar nebula. *Geochim. Cosmochim. Acta* **52**, 2841–2854.

Ireland T. R., Fegley Jr. B. (2000) The solar system's earliest chemistry: systematics of refractory inclusions. *Int. Geol. Rev.* **42** 865-894.

Krot, A. N., Scott R. D., and Zolensky M. E. (1995) Mineralogical and chemical modification of components in CV3 chondrites: Nebular or asteroidal processing. *Meteoritics* **30**, 748-775.

Krot, A. N., Yurimoto, H., Hutcheon, I. D., Glenn, J. & MacPherson, G. J. (2005) Chronology of the early Solar System from chondrule-bearing calcium-aluminium-rich inclusions. *Nature* **434**, 998-1001.

Lodders, K. (2003) Solar system abundances and condensation temperatures of the elements. *Astrophys. J.*, **591**, 1220-1247.

Luck, J.M., Allegre, C.J. (1983) Re-187–Os-187 systematics in meteorites and cosmochemical consequences. *Nature* **302**, 130–132.

Lugmair G. W. and Galer S.J.G. (1992) Age and isotopic relationships among the angrites Lewis Cliff 86010 and Angra dos Reis. *Geochim Cosmochim Acta* **56**, 1673-1694.

MacPherson G. J. and Davis A. M. (1994) Refractory inclusions in the prototypical CM chondrite, Mighei. *Geochim Cosmochim Acta* **58**, 5599–5625.

MacPherson G. J., Davis A. M., and Zinner E. K. (1995) The distribution of aluminum-26 in the early Solar System - a reappraisal. *Meteoritics* **30**, 365–386.

MacPherson G. J. (2003) *in Meteorites, Planets, and Comets, Vol. 1, Treatise on Geochemistry* (HD Holland, KK Turekian eds) (Oxford: Elsevier-Pergamon), 201-246.

MacPherson G.J., Huss G.R., and Davis A.M. (2003) Extinct 10 Be in Type A Calcium-Aluminum-Rich Inclusions from CV chondrites. *Geochim. Cosmochim. Acta* **67**, 3165-3179.

Martin P. M. and Mason B. (1974) Major and trace elements in the Allende meteorite. *Nature* **249**, 333–334.

Mason B. and Martin P. M. (1974) Minor and trace element distribution in melilite and pyroxene from the Allende meteorite. *Earth and Planetary Science Letters* **22**, 141-144.

Mason B. and Martin P. M. (1977) Geochemical differences among components of the Allende meteorite. *Smithson. Contrib. Earth Sci.* Smithsonian Institution Press, Washington, DC, vol. 19, 84–95.

Mason B. and Taylor S. R. (1982) Inclusions in the Allende meteorite. *Smithson. Contrib. Earth Sci.* **25**, 1–30.

McSween H. Y. (1977) Chemical and petrographic constraints on the origin of chondrules and inclusions in carbonaceous chondrites. *Geochim. Cosmochim. Acta* **41**, 1843-1860.

McSween H.Y. (1977) Petrographic variations among carbonaceous chondrites of the Vigarano type. *Geochim Cosmochim Acta* **41**, 1777-1790.

McSween H. Y. (1999) *Meteorites and Their Parent Planets*. New York: Cambridge University Press.

Misawa K. and Nakamura N. (1996) Origin of refractory precursor components of chondrules from carbonaceous chondrites. In Chondrules and the Protoplanetary Disk (R. H. Hewins *et al.*, eds.), pp. 99-105. Cambridge Univ., Cambridge.

Morris M.A. and Desch S.J. (2010) Thermal histories of chondrules in solar nebula shocks. *Astrophys. J.*, **722**, 1474-1494.

Mughabghab S. F. (2003) Thermal neutron capture cross sections resonance integrals and G-factors. INDC(NDS)-440.

Niederer F.R., Papanastassiou D. A., and Wasserburg G. J. (1981) The isotopic composition of titanium in the Allende and Leoville meteorites. *Geochim. Cosmochim. Acta* **45**, 1017-1031.

Nier, A.O. (1950) A redetermination of the relative abundances of the isotopes of carbon, nitrogen, oxygen, argon, and potassium. *Phys. Rev.* **77**, 789–793.

Palme, H. and Wlotzka, F. (1976) A metal particle from a Ca,Al-rich inclusions from the meteorite Allende, and the condensation of refractory siderophile elements. *Earth Planet. Sci. Lett.* **33**, 45-60.

Palme, H., Hutcheon, D., and Spettel, B. (1993) Composition and origin of refractory-metal-rich assemblages in Ca,Al-rich Allende inclusion. *Geochim. Cosmochim. Acta* **58**, 495-513.

Papanastassiou D. A., Ngo H. H., and Wasserburg G. J. (1987) Sm-Nd systematics in coarse-grained refractory inclusions from Allende. *Lunar Planet. Sci. Conf.* **XVIII**, 760–761.

Petaev M. I. and Wood J. A. (2005) Meteoritic constraints on temperatures, pressures, cooling rates, chemical compositions, and models of condensation in the solar nebula. In Chondrites and the Protoplanetary Disk, vol. 341 (eds. A. N. Krot, E. R. D. Scott and B. Reipurth). ASP Conference Series, pp. 373–407.

Podosek F. A., Zinner E. K., MacPherson G. J., Lundberg L. L., Brannon J. C., and Fahey A. J. (1991) Correlated study of initial $^{87}\text{Sr}/^{86}\text{Sr}$ and Al-Mg isotopic systematics and petrologic properties in a suite of refractory inclusions from the Allende meteorite. *Geochim. Cosmochim. Acta* **55**, 1083–1110.

Reisberg, L., Dauphas, N., Luguet, A. *et al.* (2009) Nucleosynthetic osmium isotope anomalies in acid leachates of the Murchison meteorite. *Earth Planet. Sci. Lett.* **277**, 334-344.

Rubin A.E., Wasson J.T. (1987) Chondrules, matrix and coarse-grained chondrule rims in the Allende meteorite: Origin, interrelationship and possible precursor components. *Geochim. Cosmochim. Acta* **51**, 1923-1937.

Sanders I. S. (1996) A chondrule-forming scenario involving molten planetesimals. In Chondrules and the Protoplanetary Disk (R. H. Hewins *et al.*, eds.), pp. 327–334. Cambridge Univ., Cambridge.

Scott E.R.D., Barber D.J., Alexander C.M.O., Hutchison R., Peck J.A. (1988) Primitive material surviving in chondrules: matrix. In Meteorites and the Early Solar System (J.F. Kerridge & M.S. Matthews eds.) pp. 718-745. University of Arizona Press.

Shirey S. B. and Walker R. J. (1995) Carius tube digestion for low blank rhenium-osmium analysis. *Anal. Chem.* **67**, 2136-2141.

Shu F. H., Shang H., Glassgold A. E., and Lee T. (1997) X-rays and fluctuating X-winds from protostars *Science* **277**, 1475-1479.

Shu F. H., Shang H., Gounelle M., Glassgold M., and Lee T. (2001) The origin of chondrules and refractory inclusions in chondritic meteorites. *Astrophys. J.*, **548**, 1029–1050.

Smoliar M. I., Walker R. J., and Morgan J. W. (1996) Re-Os ages of group IIA, IIIA, IVA, and IVB iron meteorites. *Science* **271**, 1099–1102.

Tatsumoto M., Unruh D. M., and Desborough G. A. (1976) U-Th-Pb and Rb-Sr systematics of Allende and U-Th-Pb systematics of Orgueil. *Geochim. Cosmochim. Acta* **40**, 617–634.

Taylor S. R. (2001) *Solar System Evolution, A New Perspective*, 2nd edn. Cambridge University Press, Cambridge.

Urey H. C. and Craig H. (1953) The composition of the stone meteorites and the origin of the meteorites. *Geochim. Cosmochim. Acta*, **4**, 36–82.

Van Schmus W. R. and Wood, J. A. (1967). A chemical-petrologic classification for the chondritic meteorites. *Geochim. Cosmochim. Acta* **31**, 747–765.

Vanhala H.A. and Boss, A.P. (2002) Injection of Radioactivities into the Forming Solar System. *Astrophys. J.* **575**, 1144-1150.

Wadhwa, M., Russell, S. S. (2000) Timescales of Accretion and Differentiation in the Early Solar System: the Meteoritic Evidence. In Protostars and Planets IV (V. Mannings, A. P. Boss, & S. S. Russell eds) Univ. Arizona Press, 995.

Walker R.J., Horan M.F., Morgan J.W., Becker H., Grossman J.N., and Rubin A.E. (2002) Comparative ^{187}Re - ^{187}Os systematics of chondrites: Implications regarding early solar system processes. *Geochim. Cosmochim. Acta* **66**, 4187-4201.

Wänke H., Baddehausen H., Palme H., and Spettel B. (1974) On the chemistry of the Allende inclusions and their origin as high temperature condensates. *Earth Planet. Sci. Lett.* **23**, 1-7.

Wark D.A. (1986) Evidence for successive episodes of condensation at high temperature in a part of the solar nebula. *Earth Planet. Sci. Lett.* **77**, 221-242.

Wark D.A. (1987) Plagioclase-rich inclusions in carbonaceous chondrite meteorites: Liquid condensates? *Geochem. Cosmochim. Acta* **51**, 221-242.

Wielandt D., Nagashima K., Krot A.N., Huss G.R., Ivanova M.A., and Bizzaro M. (2012) Evidence for multiple sources of ^{10}Be in the early solar system. *Astrophys. J.* **748**, L25.

Wood J. A. (1963) Chondrites and chondrules. *Sci. Am.*, **65**, 65–83.

Xiong Y. and Wood S. A. (1999) Experimental determination of the solubility of ReO_2 and the dominant oxidation state of rhenium in hydrothermal solutions. *Chem. Geol.* **158**, 245–256.

Yokoyama, T., Rai, V.K., Alexander, M.O., Lewis, R.S., Carlson, R.W., Shirey, S.B., Thiernens, M.H., and Walker, R.J. (2007) Osmium isotope evidence for uniform distribution of s- and r process components in the early solar system. *Earth Planet. Sci. Lett.* **259**, 567–580.

Yokoyama, T., Walker, R.J., Alexander, C.M.O'D., MacPherson, G.J. (2009) Osmium isotope anomalies in chondrite components: refractory inclusions, chondrules, metal and presolar grains. *Lunar Planet. Sci. XL*, 1489.

Yoneda S. and Grossman L. (1995) Condensation of $\text{CaO}-\text{MgO}-\text{Al}_2\text{O}_3-\text{SiO}_2$ liquids from cosmic gases. *Geochim. Cosmochim. Acta* **59**, 3413-3444.